MODELING THE IMPACT ON SEDIMENT TEXTURE OF LARGE-SCALE TIDAL POWER IN THE BAY OF FUNDY

by

Shaun Gelati

Submitted in partial fulfillment of the requirements
for the degree of Master of Science

at

Dalhousie University
Halifax, Nova Scotia
November 2012

DALHOUSIE UNIVERSITY

DEPARTMENT OF OCEANOGRAPHY

The undersigned hereby certify that they have read and recommend to the Faculty of Graduate Studies for acceptance a thesis entitled "MODELING THE IMPACT ON SEDIMENT TEXTURE OF LARGE-SCALE TIDAL POWER IN THE BAY OF FUNDY" by Shaun Gelati in partial fulfillment of the requirements for the degree of Master of Science.

Dated: November 30, 2012

External Examiner: _____
Mr. Timothy G. Milligan

Supervisor: _____
Dr. Paul S. Hill

Readers: _____
Dr. Jinyu Sheng

_____
Dr. Keith R. Thompson

DALHOUSIE UNIVERSITY

DATE: November 30, 2012

AUTHOR: Shaun Gelati

TITLE: MODELING THE IMPACT ON SEDIMENT TEXTURE OF LARGE-SCALE TIDAL POWER IN THE BAY OF FUNDY

DEPARTMENT OR SCHOOL: Department of Oceanography

DEGREE: M.Sc. CONVOCATION: May YEAR: 2013

_____

Signature of Author

"Réfléchissez au mouvement des vagues, au flux et au reflux, au va-et-vient des marées, l'océan est une immense force perdue."

Victor Hugo

TABLE OF CONTENTS

LIST OF TABLES

LIST OF FIGURES

ABSTRACT

The output of a 3-D ocean circulation model and information on nearly 10,000 sediment samples are used to examine the extent to which a model of ocean currents can be used to predict seabed sediment texture in the Bay of Fundy and Gulf of Maine. It is found that sediment texture is generally closer to equilibrium with maximum tidal bed shear stress in the Gulf of Maine than in the Bay of Fundy. In the Bay of Fundy, competent mean grain sizes are generally coarser than observed mean grain sizes, and further interpretation suggests that sediment supply has a dominant influence on texture. Furthermore, the impact on texture is predicted for two tidal power development scenarios in the Minas Passage (*Hasegawa et al.*, 2011). For a 2.0 GW of power scenario, a sediment fining is predicted in parts of Minas Passage, although the impact should be small as supply dominates texture. Further research is needed to quantify with more precision the potential impact of tidal power development on texture, especially in the Bay of Fundy.

List of Abbreviations and Symbols Used

Abbreviation	Description
USGS	United States Geological Survey
GSC	Geological Survey of Canada
BIO	Bedford Institute of Oceanography
POM	Princeton Ocean Model
ADCP	acoustic Doppler current profiler
FORCE	Fundy Ocean Research Center for Energy

Symbol	Description	Units
τ_c	particle critical erosion shear stress	Pa
$\tau_c^\star$	dimensionless particle critical erosion shear stress	none
ρ_s	sediment density	kg m^{-3}
ρ	seawater density	kg m^{-3}
g	gravitational acceleration	m s^{-2}
D	sediment particle diameter	m
$R_c^\star$	critical particle Reynolds number	none
$u_c^\star$	critical shear velocity	m s^{-1}
ν	seawater kinematic viscosity	m^2 s^{-1}
D_{50}	median sediment particle diameter	m
ϕ	sediment particle size on the phi scale	none
D_0	reference sediment particle diameter	mm
σ	sigma-coordinate in the vertical	none
z	vertical coordinate	m
η	sea-surface elevation	m
H	water depth	m
T	temperature	°C
U	instantaneous horizontal speed	m s^{-1}

Symbol	Description	Units
V	instantaneous horizontal speed	m s^{-1}
W	instantaneous vertical speed	m s^{-1}
D_{mean}	sediment particle mean diameter	m
τ_0	instantaneous bed shear stress	Pa
x	horizontal coordinate	variable
y	horizontal coordinate	variable
C_D	drag coefficient	none
κ	von Kármán constant	none
z_0	roughness parameter	m
k_s	bed roughness length scale	m
α	grain geometry parameter	none
ϕ_0	sediment particle angle of repose	$^\circ$
β	seabed inclination	$^\circ$
$R_\star$	bed roughness Reynolds number	none
$u_\star$	shear velocity	m s^{-1}
$\hat{Z}_k$	variable's interpolated value	variable
P	predicted variable	variable
O	observed variable	variable
n	number of instances in variables O and P	none
R^2	coefficient of determination between O and P	none
ϵ_M	mean absolute gross error between O and P	none
$\bar{\tau_0}$	residual bed shear stress magnitude	Pa
T_s	model simulation period	s

ACKNOWLEDGEMENTS

Foremost, I would like to thank Paul Hill, my supervisor, for making this thesis possible with his advice, enthusiasm, patience, and understanding. I thank Jinyu Sheng and Keith Thompson, my advisory committee, for their advice, and interest in the project. I also acknowledge the Monday "group support" of the Particles Lab.

On a more technical note, I would like to thank Daisuke Hasegawa, for providing the ocean circulation model data, and Christopher Veinot, for putting together the sediment data. I also acknowledge the help of Simon Higginson, with mapping and interpolation, and the advice of Stephanie Kienast, on the many aspects of writing a thesis.

Last but not least, I would like to thank my family, for their moral support many kilometers away, and friends in Halifax, who have provided the much needed good times one needs when completing studies in general. My family is: Maman, David, Eve-Lyn, Pierre-Olivier, Grand-Papa and Grand-Maman, Michel G., Christine, Roxane, Michel D. and Johanne. The friends are: Teto, Andrew, Tara, Karl and Christiane, Anna, J-P and Fran, Jenna, Mat and Alexandra, Justine, Jessica, Nina, Myriam, Eric, Jorge, Shiliang, Will, Mike B., Mat B., Harold, Øyvind, and Jing. Many other people in the Department of Oceanography at Dalhousie, and outside, have made my time in Halifax enjoyable. My thanks go to those also.

Financial support was provided by the Ocean Energy and Environment Research Association (OEER), the Natural Sciences and Engineering Research Council of Canada (NSERC), and Dalhousie University.

CHAPTER 1

INTRODUCTION

The strong currents induced by the tides make the Bay of the Fundy a promising region for tidal power development. In the Bay of Fundy and Gulf of Maine, tidal near-bed currents are known to be an important influence for sediment texture, and *Hasegawa et al.* (2011) has shown that large-scale tidal power in the Bay of Fundy would likely have an impact on tidal circulation in the whole Bay of Fundy and Gulf of Maine. Tidal power generation therefore may have an impact on sediment texture. Little is known about the impact that large-scale tidal power may have on sediment texture on regional scales. This is especially true for resonant systems like the Bay of Fundy and Gulf of Maine. The resonant nature of the system means that impact on tidal circulation in part of the region could have consequences for its remainder.

A potential impact on sediment texture distribution is of ecological and economic importance, and this impact needs to be assessed. Sediment texture on the floor of the ocean is an important aspect of benthic ecosystems and their productivity, as they provide spawning grounds and food to many animals (*Methratta and Link*, 2006). Fisheries are dependent on this productivity, and fisheries represent the livelihood of many coastal human communities.

There are mainly two basic modeling approaches to predict the impact of tidal power on sediment texture. The first one makes use of the concept of competent grain size (*Buffington and Montgomery*, 1999). The competent grain size is the largest particle size that a flow is capable of mobilizing. If the seabed texture is in equilibrium with the near-bed flow, one can use the flow competence to predict a change in grain size that would result from a change in flow. This represents a simpler approach than a second approach to

modeling sediment texture, which is a coupled ocean circulation and sediment transport model (*Blaas et al.*, 2007; *Warner et al.*, 2008).

It is often assumed that on geological time scales, regional transport pathways lead to an equilibrium between the near-bed flow field and sediment texture. Although this idea has been put forth on qualitative grounds for the Bay of Fundy and Gulf of Maine region (*Emery and Uchupi*, 1972), it remains to be validated quantitatively. The present thesis' main aims are to examine if there is equilibrium between near-bed tidal flow and sediment texture, and subsequently use this knowledge in assessing the impact of large-scale tidal power in the Bay of Fundy.

1.1 Background

1.1.1 Impact of Large-Scale Tidal Power

The Bay of Fundy and Gulf of Maine are situated offshore of the northeastern coast of the North-American continent. The Gulf of Maine is a large, deep (maximum depth of $\sim$ 300 m) embayment, which extends from Cap Cod in the southwest to Grand Manan Island in the northeast. This embayment is $\sim$ 600 km in length and $\sim$ 500 km in width. The Gulf of Maine's seafloor has several basins in its inner part and banks mostly in its outer part towards the Atlantic Ocean. Major basins are Murray, Jordan and Georges Basins, and major banks are Georges, Browns and Stellwagen Banks (Figure 1.1). The Bay of Fundy can be considered a tidal channel of considerable dimensions, i.e. $\sim$ 300 km in length and $\sim$ 100 km in width at its entrance, or lower part. At its head are Chignecto Bay and the Minas Basin, or upper Bay of Fundy, the latter basin being connected to the lower Bay of Fundy by the Minas Channel.

Figure 1.1 *(following page)*: Map of sub-regions of the Bay of Fundy and Gulf of Maine region. Upper panel is the whole region and lower panel is a close-up of the Minas Basin region. Sub-regions of the Bay of Fundy are: lower Bay of Fundy (LBF), upper Bay of Fundy (UBF), Minas Channel (MC), Minas Passage (MP), Minas Basin (MB), Cobequid Bay (COB), Avon River (AR), Northern Bight (NB) and Chignecto Bay (CHB). Sub-regions of the Gulf of Maine are: Cape Cod Bay (CCB), Merrimack River (MR), Penobscot Bay (PSB), Grand Manan Island (GMI), Passamaquoddy Bay (PAB), Murray Basin (MBS), Jordan Basin (JB), Georges Bank (GBA), Georges Basin (GBS), eastern Gulf of Maine (EGM), Scotian Shelf (SS), Browns Bank (BB) and Scotian Slope (SSL). Isobaths are in m.

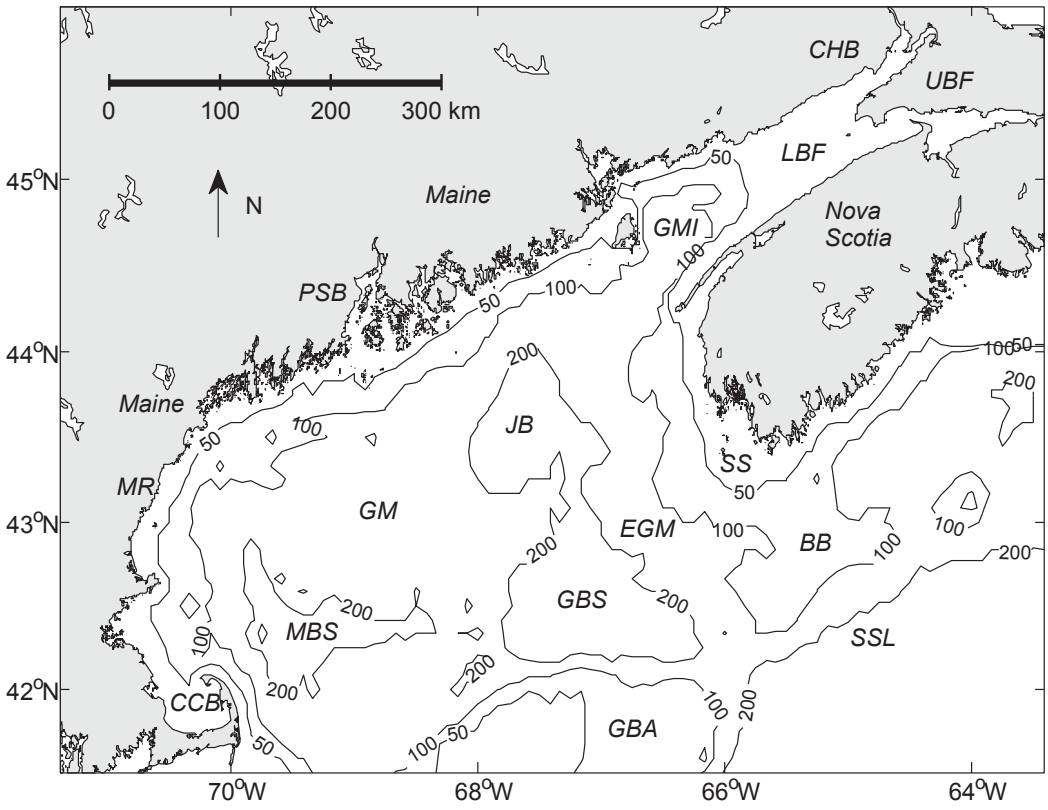
0
100
200
300 km
N
CHB
UBF
LBF
Nova
Scotia
GMI
Maine
PSB
Maine
MR
JB
SS
GM
EGM
BB
GBS
MBS
SSL
CCB
GBA
50
100
200
45°N
44°N
43°N
42°N
70°W
68°W
66°W
64°W

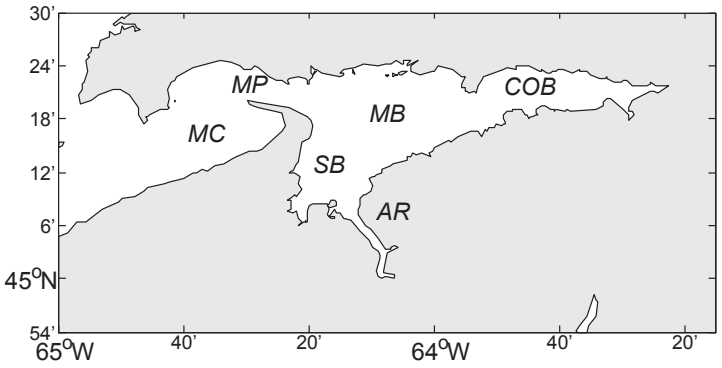
MP
COB
MB
MC
SB
AR
30'
24'
18'
12'
6'
45°N
54'
65°W
40'
20'
64°W
40'
20'

Strong currents make the Bay of the Fundy a promising region for tidal power development. Currents of up to 5 m s^{-1} have been measured in the Minas Passage. Recently, *Hasegawa et al.* (2011) estimated the tidal power potential to be 7.6 GW in the Minas Passage alone (Figure 1.1). The Bay of Fundy is home to the highest tides in the world. The Bay of Fundy and Gulf of Maine system, which has an intrinsic oscillation period of 13.3 h, is mainly forced by the lunar tides at a period of 12.42 h (M_2 tidal constituent). This system and the forcing tides are thus close to resonance and this causes the high tides observed in the region (*Garrett*, 1972).

A few studies have been done on tidal barrages in the Bay of Fundy and the potential impact on the surrounding physical environment as far as the Gulf of Maine. *Garrett* (1972) is the first author to recognize that the impact could be this far-reaching. *Garrett* (1972) hypothesized that a tidal dam, also known as a barrage, in the upper Bay of Fundy would likely push the Bay of Fundy and Gulf of Maine system closer to resonance with the M_2 tides. This would in turn increase tidal elevations in most of the Gulf of Maine. This increase in tidal elevations for the Gulf of Maine, but also for the lower Bay of Fundy, has been estimated and confirmed by recent studies (*Karsten et al.*, 2008; *Hasegawa et al.*, 2011). Up until recently, tidal power development globally has been done mainly with tidal dams. The Annapolis Tidal Power Plant is an example in Annapolis Royal, Nova Scotia. Consequently, most studies of the impact of tidal power in the Bay of Fundy and Gulf of Maine have focused on the impact this last type of construction would have. These studies have investigated the impact of tidal power on tidal circulation and elevations (*Greenberg*, 1979; *Sucsy et al.*, 1993), and suspended sediment concentration (*Greenberg and Amos*, 1981). No other tidal power projects have been pursued in the Bay of Fundy after the 20-MW Annapolis Royal tidal dam.

Recent developments in tidal power technology have created a need to reevaluate the impact of tidal power in the Bay of Fundy and Gulf of Maine. Tidal in-stream turbines are a technology that shows promise as it offers flexibility for tidal power farm development. As opposed to tidal dams, in-stream turbine farms can vary in size and, therefore, in the impact they have on the surrounding environment. For this technology, the studies of *Hasegawa et al.* (2011) and *Karsten et al.* (2008) have estimated the available tidal resource in the upper Bay of Fundy, and the impact on tidal circulation and elevations in the Bay of Fundy and Gulf of Maine area.

Studies of the impact on sediment dynamics of in-stream turbines have been made in other parts of the world (*Neill et al.*, 2009, 2011). These studies have shown the importance of assessing the far-field impact of such devices on sediment dynamics. For example, *Neill et al.* (2011) have shown that a 300-MW tidal turbine farm could have a significant impact on the sediment dynamics of the Alderney Race, United Kingdom. A 2-D numerical ocean circulation model was used for this assessment. Depth-averaged speeds could be affected by as much as ~ 0.05 m s^{-1} in a radius of ~ 10 km from the energy extraction sites. At these sites, depth-averaged speeds should be mainly reduced, and increases are predicted away from these sites. More specifically, *Neill et al.* (2011) found that such a development could impact bed level changes of the South Banks by as much as 10 % over a spring-neap cycle. This impact needs to be compared to seabed level natural variability (inter-annual and inter-seasonal) to determine if there is need for mitigation.

Studies on the potential impact on sediment dynamics of large-scale development of this type of technology in the Bay of Fundy and surrounding areas have yet to be done. Because of the resonant nature of Bay of Fundy and Gulf of Maine system, the assessment of the impact of potential power development in a part of the system must be done for the entire system. *Li* (2011) noted that better knowledge of the present-day sediment dynamics in the Bay of Fundy is needed before an impact assessment is done. More specifically, more data on sand transport, waves, and the ocean circulation are needed in order to better calibrate modeling efforts of sediment dynamics (*Li and Heffler*, 2002). Notable modeling and observational efforts have recently been made toward this objective (*Li et al.*, 2010; *Todd et al.*, 2010; *Wu et al.*, 2011).

1.1.2 Sediment Dynamics of the Bay of Fundy and Gulf of Maine

Knowledge of sediment dynamics of the Bay of Fundy and Gulf of Maine has evolved with methods of inquiry. Up until the 1970s, the seafloor sediment distribution of the Bay of Fundy and Gulf Maine had been mainly studied with mechanical means such as grabs and corers. An account of the sediment sampling done in the region prior to that period is the review of *Emery and Uchupi* (1972). The account of *Emery and Uchupi* (1972) has highlighted that the Bay of Fundy and Gulf of Maine's basement is overlain by sediments that are diverse in age and origins. These sediments are a mixture of relict and modern sediments, with glacial, fluvial and coastal plain origins. The thickness of Holocene (past ~ 10 kyr) and Quaternary (past ~ 2.5 Myr) sediments in the Cape Cod

Bay area can measure more than 40 and 100 m, respectively. The basins of the Gulf of Maine are an area where Holocene sediments are generally 40 m thick or more. In the Bay of Fundy, the Scotian Shelf and Georges Bank, Holocene sediments are thinner, with thicknesses up to 1 m. In some areas, Holocene sediments are often absent and the underlying Quaternary sediments, with thicknesses generally $\sim$ 20 m on the Scotian Shelf and up to 60 m in the Georges Bank area, are exposed. Furthermore, *Emery and Uchupi* (1972) sum up the present-day sediment dynamics of the Bay of Fundy and Gulf of Maine region as follows: relict sediment superposition by modern fines on the one hand, and relict sediments adjusting to modern near-bed flow conditions through winnowing of their relict fines on the other hand.

The refinement of sonar technology in the 1970s enabled investigators to study seafloor sediments with increased spatial resolution. The study of *Fader et al.* (1977) on the lower Bay of Fundy, eastern Gulf of Maine and Scotian Shelf surficial sediment distribution made intensive use of sonar technology. However, samples of the region's seafloor sediments were still necessary to calibrate the result of the sonar surveys. More recently, the usSEABED database (*Reid et al.*, 2005) has been assembled by the United States Geological Survey. The usSEABED database is a digital collection of surficial sediment samples made in American coastal waters over approximately the last century.

The end of the 1970s witnessed the emergence of a new type of field study in the Bay of Fundy and Gulf of Maine region: the study of the dynamics of sediments under the action of near-bed currents. Before that period, understanding of sediment dynamics was based on interpretation of seabed textural parameters (*Fader et al.*, 1977). For example, the interpretation for the coarse, poorly-sorted sediments of the Scotian Shelf was that finer sediments had been simply winnowed away. Strong tidal near-bed currents have removed Holocene-aged sediments, and have exposed the poorly sorted glacial till (*Fader et al.*, 1977). Furthermore, these finer sediments were the source material for the surficial sheets of mud and sand observed in the lower Bay of Fundy. The emergence of in situ current meters and turbidity sensors allowed direct observations of sediment dynamics (*Allen*, 1971; *Lambiase*, 1980). The study of *Twichell* (1983) on Georges Bank used near-bed current-meter observations to link the dynamics of sediment and bedforms to the strong tidal currents present in the region. The calculation of residual currents from the same current-meter observations led to insights on the causes of the juxtaposition of fine and

coarse-grained sediments on Georges Bank.

Since the 1980s, computers and numerical ocean circulation models have widened the scope of studies on regional sediment dynamics (*Uncles*, 1983). Observations of near-bed currents were scarce in the 1980s. Numerical models provided a means to estimate these. Furthermore, models could estimate these near-bed currents with a spatial extent still unmatched by observational studies today. *Amos and Judge* (1991) noted that sand transport is evident on the Canadian continental shelf from the wide-spread presence of sorted sand. They also noted that fine material transport is evident on the Canadian continental shelf from the wide-spread presence of ponded fine-grained sediments in basins. The use of a numerical model then enabled *Amos and Judge* (1991) to estimate the vectors of bedload sand transport under various meteorological conditions in this region. *Amos and Judge* (1991) concluded that there is general agreement that two sediment transport regimes coexist in the Bay of Fundy and Gulf of Maine area. The Gulf of Maine basins are areas of fine-grained sediment deposition made possible by the weak currents that prevail in this region. Intermitent bedload transport of coarser-grained sediments by strong tidal currents characterizes the regime prevailing over Georges Bank, the Scotian Shelf and the Bay of Fundy.

Recent studies with numerical models in the Bay of Fundy have quantified tidally-dominated sediment transport. *Wu et al.* (2011) used a high-resolution 3-dimensional (3-D) numerical model forced by several tidal constituents to study bedload and suspended sediment transports in the Minas Basin. The total (bedload and suspended load) transport, averaged over a tidal cycle (net), was found to form a counter-clockwise gyre in the Minas Channel, and to be directed eastward in the Minas Passage and western Minas Basin. These patterns are generally the same for individual bedload and suspended transport. In the Minas Passage, maximum mean bottom shear stress was found to be ~ 20.0 Pa during flood tide. High bed shear stresses during flood tide contribute to net total transports between 0.1–0.2 kg m^{-1} s^{-1} directed eastward in the Minas Passage. The transport patterns can be considered more robust than the actual transport magnitudes, as the latter are strongly sensitive to model parameters. For the Canadian Atlantic shelf, *Li et al.* (2010) used a numerical model similar to the study of *Wu et al.* (2011), but included wave climatology for the calculation of near-bed currents and associated sediment transport. *Li et al.* (2010)

found that seabed disturbance is dominated by the tides in the Bay of Fundy and is wave-dominated on the inner Scotian Shelf. Sediment is mobile up to a 100 % of the time over large areas of the Bay of Fundy under the action of tidal currents. On the other hand, waves mobilize sediment up to 30 % of the time on some of the banks of the Scotian Shelf.

Over the years, studies done in the Bay of Fundy and Gulf of Maine region have shown that tidally-induced sediment transport is widespread and frequent in the region. A general assumption is that this transport eventually leads a sediment distribution to obtain equilibrium with the dominant near-bed flow. This statement from *Loring* (1979) exemplifies well the assumption for the Bay of Fundy: "*A Pleistocene glacial drift cover has been reworked to form extensive thin deposits of gravel, sand, and mud in hydraulically suitable locations*." In the Bay of Fundy and Gulf of Maine, the two present-day modern sediment dynamics regimes described by *Emery and Uchupi* (1972) are this equilibrium. This idea, though, remains to be quantitatively validated. Only modeling can provide relevant information both on long timescales and at the regional scale (*Dufois et al.*, 2008). Modeling would then be useful in a vast area such as the Bay of Fundy and Gulf of Maine to compare modeled stress with observed seabed texture. Given the many and spatially extensive observational and modeling efforts than have been done over the last century in the area, it is possible to examine explicitly the hypothesis that sediment texture is in equilibrium with seabed stress. Furthermore, the validation of the idea would inform the approach to take for the assessment of the impact of tidal power in the Bay of Fundy on sediment texture.

1.1.3 Sediment Texture and Near-Bed Hydrodynamics

Near-bed currents at the regional scale can be generated by waves, winds, tides and density differences. The magnitude and associated frequency of occurrence of near-bed currents generated by these processes vary in space and time. While for long-term transport it is generally assumed that frequency of events determines net transport pathways (*Porter-Smith et al.*, 2004), for sediment texture it is the magnitude (*Signell et al.*, 2000). In the coastal environment, long-term transport of sediments and texture is usually dominated by one process. For example, *Porter-Smith et al.* (2004) calculated the frequency with which modeled wave-generated and tidal bed shear stresses exceed the estimated critical erosion shear stress of the sediment distribution on the Australian Continental Shelf. Based on this work, they classified the Autralian Continental Shelf into wave- and tide-dominated

regions. In most of the Bay of Fundy and Gulf of Maine, tides are known to be a dominant determinant of sediment transport; on the Scotian Shelf, storm-generated waves dominate transport in marginal, shallow, coastal areas, and shallow banks (*Amos and Judge*, 1991; *Li*, 2011).

If the magnitude of the largest near-bed currents determines sediment texture, then the former can be used to predict the latter, and vice versa. This is the rationale used in the common, simple approach of comparing the near-bed flow and observed sediment texture (*Jewell et al.*, 1993; *Porter-Smith et al.*, 2004; *Signell et al.*, 2000). On the Australian Continental Shelf, this hydraulic equilibrium is referred to explicitly when *Porter-Smith et al.* (2004) assert that swell waves and tidal currents winnow away fine sediments to expose coarser sediments. In the study of *Signell et al.* (2000) in Long Island Sound, this equilibrium is referred to implicitly, as a relationship is sought between tidal near-bed currents and sediment texture.

The concept of a sediment texture that is in equilibrium with the local hydrodynamic stress is encapsulated in the concept of the competent grain size (*Buffington and Montgomery*, 1999). The competent grain size is the largest particle that can be moved at a given stress. At a threshold termed critical shear stress (τ_c), motion of sediment particles is initiated and transport occurs. A pioneering study on critical shear stress is that of *Shields* (1936). Based on sediment transport data collected with a bed of constant particle size sheared by a unidirectional flow, *Shields* (1936) built what is widely known now as the Shields diagram (Figure 1.2). The Shields diagram enables one to determine the shear stress necessary to set in motion sediment particles of various sizes. In such a diagram, the critical shear stress $\tau_c^\star$ is expressed in non-dimensional form as

$$\tau_c^\star = \frac{\tau_c}{(\rho_s - \rho)gD}, \tag{1.1}$$

where ρ_s is the sediment particle's density, ρ is the seawater density, g is the gravitational acceleration (g = 9.8 m s^{-2}) and D the sediment particle diameter. $\tau_c^\star$ is then made to depend on the flow regime, which is characterized by the critical particle Reynolds number

$$R_c^\star = \frac{u_c^\star D}{\nu}, \tag{1.2}$$

where $u_c^\star$ is the critical shear velocity, which is $u_c^\star = (\tau_c/\rho)^{0.5}$, and ν is the kinematic

viscosity. Many studies similar to *Shields* (1936) have been done over the years (*Buffington and Montgomery*, 1997; *Miller et al.*, 1977). Data from various studies have been used to calibrate theoretical models of initiation of motion (*Wiberg and Smith*, 1987), and such models can be used predict the competent grain size for a given stress (see Chapter 2). Competent grain size for a stress derived from measurements or a model can be compared to observed grain size in the seabed to assess whether sediment texture is in equilibrium with that stress.

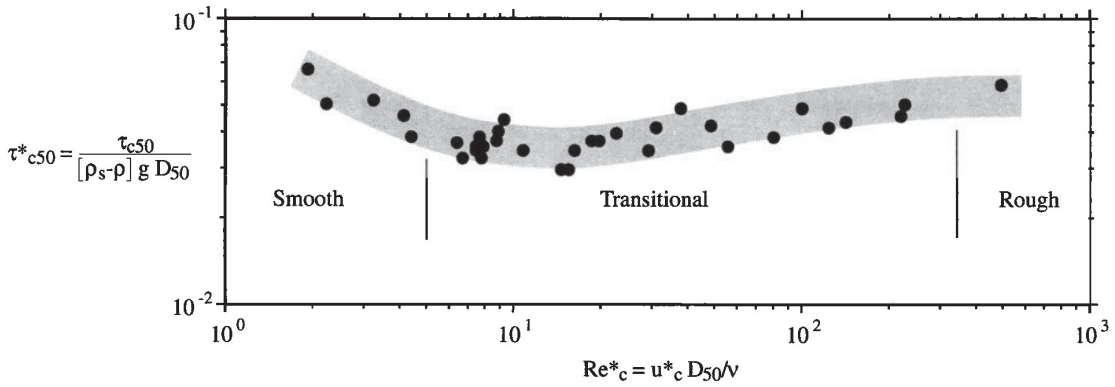

Figure 1.2: Shields diagram for a sediment mixture of median diameter D_{50} (*Buffington and Montgomery*, 1997).

Some studies take a more complex approach to study the sediment texture distribution of a specific region by using coupled ocean circulation and sediment transport models. Using such a system, *Warner et al.* (2008) were able to model the evolution of bed morphology and texture under several meteorological scenarios in Massachussets Bay. Studies that are also in this category, but less complex than coupled sediment transport models, are those that determine sediment transport vectors, and zones of transport convergence and divergence (*Bobertz and Harff*, 2004; *Dufois et al.*, 2008; *Signell et al.*, 2000). In the Bay of Fundy and Gulf of Maine, the studies of *Wu et al.* (2011) and *Amos and Judge* (1991) are some examples. To estimate sediment transport patterns, sediment transport formulas are necessary in addition to ocean circulation models. The various sediment transport formulas available in the literature do not always produce good agreement with observed transports (*Li and Heffler*, 2002). This is thought to be due in part to incomplete understanding of boundary-layer processes. Nonetheless, in the studies of *Wu et al.* (2011)

and *Amos and Judge* (1991), it is claimed that modeled transport pathways are generally robust.

1.2 Objectives

The objectives of the present thesis are to: (1) examine the equilibrium, or lack thereof, between modeled near-bed tidal currents and seabed sediment texture in the Bay of Fundy and Gulf of Maine and (2) to predict the potential impact of tidal power development scenarios on sediment texture in the Bay of Fundy and Gulf of Maine. The two objectives of this thesis are addressed primarily through the use of archived sediment data and the output of a 3-D model of tidal currents. Modeling enables the systematic and spatially extensive comparison of tidal near-bed currents with sediment texture needed to address the first objective of this thesis. Modeling also is used to address the second objective of this thesis, as little is known on the far-field impact of large-scale tidal power on sediment texture.

1.3 Structure

The structure of the present thesis is as follows. Chapter 2 details the sediment data set and the ocean circulation numerical model. Chapter 3 presents key results of the present thesis. Those results pertain to the relationship between near-bed tidal currents and surficial sediment character in the Bay of Fundy and Gulf of Maine region. Chapter 4 is a discussion on this last relationship and of the potential impact of tidal power on sediments in the Bay of Fundy and Gulf of Maine. Chapter 5 reviews the results of this thesis and suggests future work that needs to be undertaken to further address its objectives.

CHAPTER 2

METHODS

2.1 Sediment Data

Information on sediment samples from two data bases and one data set were gathered by *Veinot* (2010) to build a data set with good coverage of the Bay of Fundy and Gulf of Maine area. This study's data set contains 9357 sediment samples. Location of these samples is shown in Figure 2.1. The first data base that was used is the usSEABED data base of the United States Geological Survey (USGS). A total of 7116 samples were selected from this data base. Sampling locations include the Gulf of Maine and the Scotian Shelf. Methods of collection include different types of grabs and corers. Methods of grain size analysis include (qualitative) visual determination of samples' texture and (quantitative) analytical methods such as sieving and diffractometry. For instance, the gravel, sand, silt and clay contents of many older samples were determined visually (*Reid et al.*, 2005). From these contents, mean phi size was estimated with a systematic procedure. A margin of error is associated with this procedure and visual determination of sample's texture. It is estimated that in the usSEABED data base, the margin of error is $\pm$ 0.8 ϕ (*Reid et al.*, 2005). The second data base that was used is the Expedition data base of the Geological Survey of Canada (GSC). A total of 2118 samples were selected from this data base. These were collected in the Bay of Fundy, Gulf of Maine and Scotian Shelf over the 1950–2010 period. Different types of grabs and corers were used for collection of the samples. The data set that was used comes from the Bedford Institute of Oceanography (BIO) (Tim Milligan, personal communication). The 123 samples of this data set were collected throughout the Bay of Fundy in the years 1977 and 1994. Sample collection was done with different types

of grabs, and subsequent grain size distributions were obtained with a Coulter counter and the wet sieving method (*Milligan*, 1994; *Loring*, 1982).

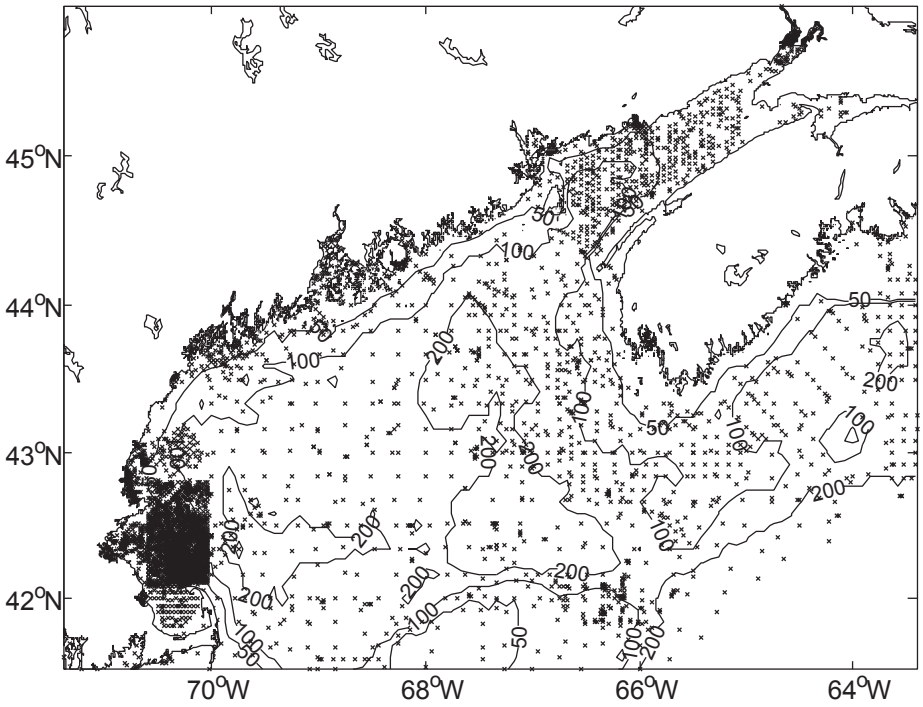

Figure 2.1: Compiled database sample locations in the Bay of Fundy and Gulf of Maine region. The region of the Gulf of Cape Cod and Massachussets Bay has undergone more sampling than other areas, although the coverage's quality (regularity and resolution of the sampling) is good for most of the Bay of Fundy and Gulf of Maine region. Isobaths are in m.

For a given sample in the dataset, generally available variables are gravel, sand, silt and clay contents (in %), and the mean, standard deviation, kurtosis and skewness of the grain size distribution. These variables describe a sample's texture. The latter four variables are referred to as textural parameters throughout this thesis. The textural parameters were calculated by converting grain diameters D (in mm) to ϕ values with the following relationship: $\phi = -\log_2(D/D_0)$, where D_0 = 1 mm, and is a reference diameter. Throughout this thesis, whenever textural parameter values are reported on the phi scale, a ϕ symbol is

put after this value. Table 2.1 shows texture equivalencies for possible ϕ values. Only the mean and standard deviation were used in this study.

Table 2.1: Textural classes and equivalencies on the ϕ scale.

Texture	Grain sizes (on ϕ scale)	Grain sizes (mm)
Clay	> 8	$< 3.9\times10^{-3}$
Silt	4 to 8	0.0625 to 3.9×10^{-3}
Sand	-1 to 4	2 to 0.0625
Gravel	-8 to -1	256 to 2
Boulder	$<$ -8	> 256

2.2 Ocean Circulation Model

An ocean circulation numerical model was developed by *Hasegawa et al.* (2011) to simulate the tidal elevations and circulation of the Bay of Fundy and Gulf of Maine area over a period of $\sim$ 30 days. This period includes two spring-neap tidal cycle. The model is based on the Princeton Ocean Model (POM). Its main characteristics are that it is 3-D and uses sigma coordinates in the vertical. Sigma coordinates are terrain-following coordinates widely used in coastal models, and are defined as $\sigma = (z - \eta)/(H + \eta)$, where z is a specified depth within the water column (negative), η is the sea surface elevation and H is the water depth (all in m). In the model, the water column is divided into 31 equal σ-levels. An advantage of this coordinate system is the higher vertical resolution in shallower regions of a domain.

The model comprises child and parent submodels that exchange information through a two-way nested-grid technique. The child submodel's domain covers the Bay of Fundy with a horizontal resolution of $\sim$ 1.5 km, while the parent submodel's domain covers the Gulf of Maine with a resolution of $\sim$ 4.5 km. In the study of *Hasegawa et al.* (2011), these different resolutions were chosen because tidal energy extraction scenarios take place in the Bay of Fundy. Water density and salinity are assumed constant throughout the domain, so the modeled ocean circulation is barotropic. The model is forced at the parent submodel open boundary by sea surface elevations and depth-mean current velocities of five tidal constituents, which are M_2, N_2, S_2, K_1 and O_1. The model's equations are discretized on an Arakawa C-grid shown in Figure 2.2, and solved with numerical methods.

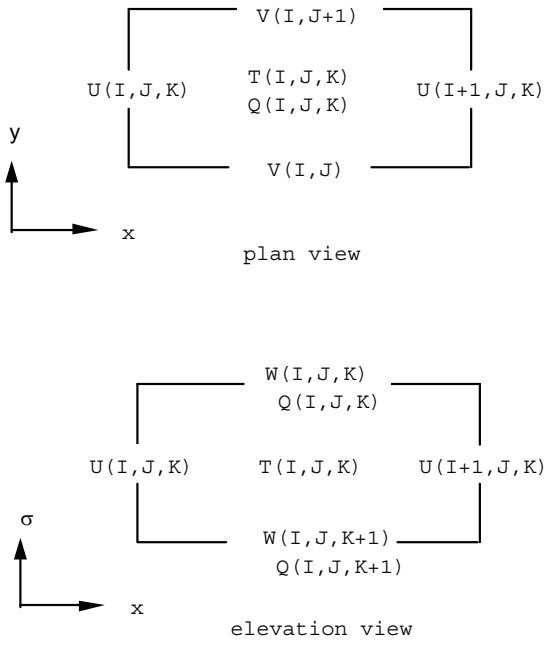

Figure 2.2: Arakawa C-grid used to discretize the model's equations (*Mellor*, 2004). In the elevation view, scalars are located at the center of grid cells. Scalars can be temperature (T here), salinity, or elevation. Vector components, on the other hand, are located at mid-distance between grid nodes. Vector components can be velocity components (U, V and W here) or bed shear stress vector components. In the elevation view, velocity components are located at mid-depth of σ-levels.

The model was validated with observations made at ten tide stations within the Bay of Fundy and Gulf of Maine region. The validation process ensures that a model output is reasonably consistent with observations. Average relative errors in amplitude (ϵ_A) and phase (ϵ_φ) are similar to those of WebTide. WebTide is the main tidal prediction model used by Fisheries and Oceans Canada. Figure 2.3 shows the M_2 tidal constituent values of amplitude and phase between the ten tide stations, Webtide and the model of *Hasegawa et al.* (2011). Furthermore, Figure 2.4 shows depth-averaged M_2 tidal ellipses produced by Webtide and the model used in this study. The model was also validated with acoustic Doppler current profiler (ADCP) measurements at three locations in the Minas Passage. Observed and modeled data are in good agreement.

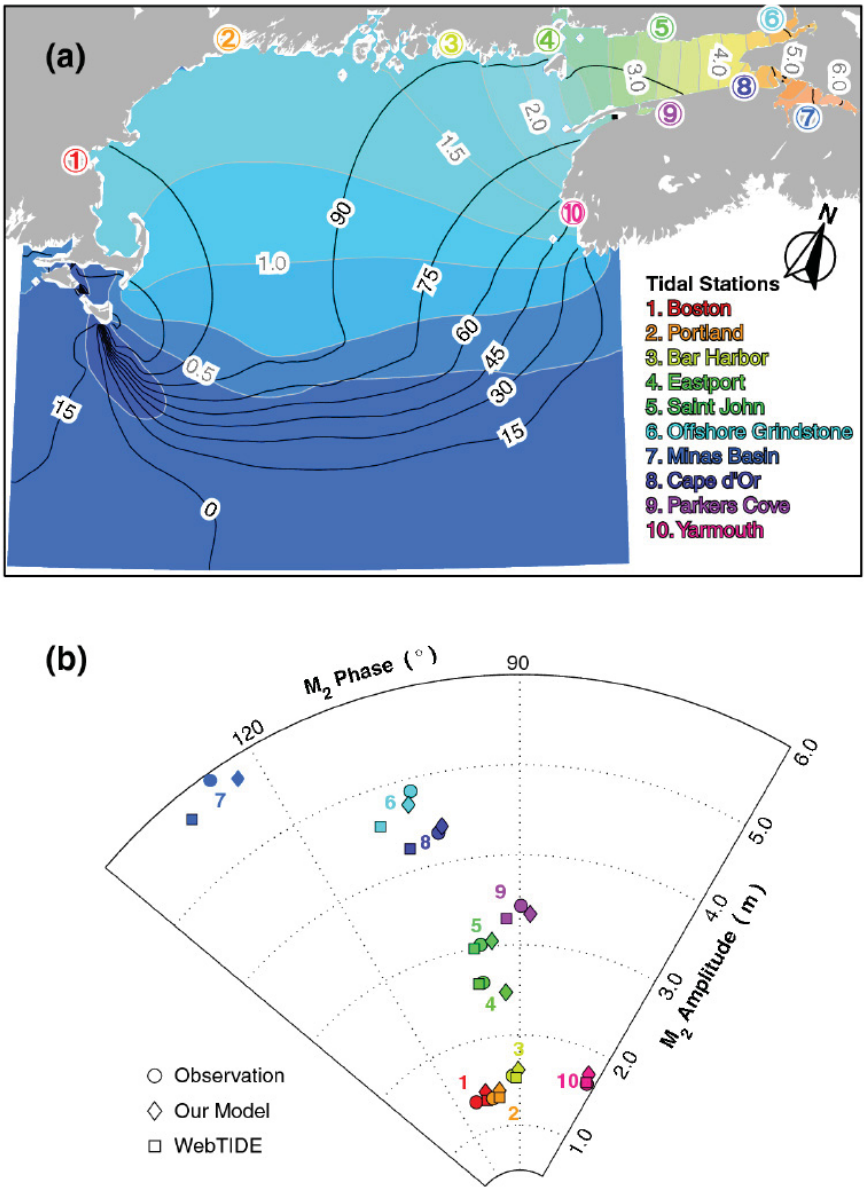

Figure 2.3: a) Map of M_2 tidal constituent amplitudes and phases produced by the model for the Bay of Fundy and Gulf of Maine region (*Hasegawa et al.*, 2011). The names of the ten tide stations are given and numbered. b) Diagram comparing the M_2 tidal constituent values of amplitude and phase. The comparison is between the ten tide stations (circles), Webtide (squares) and the model (diamonds) used in this study.

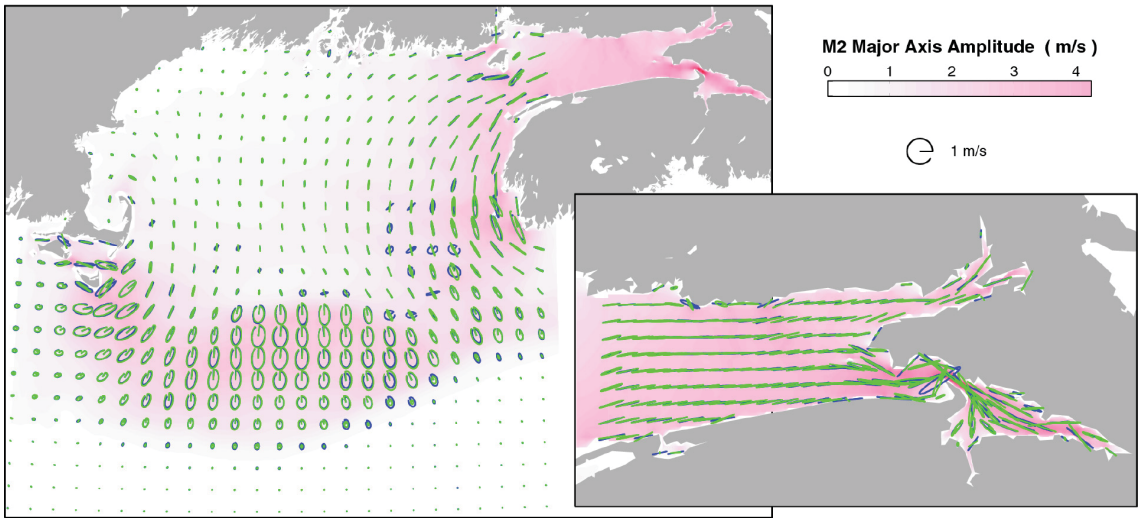

Figure 2.4: Map of depth-averaged M_2 tidal ellipses produced by Webtide (blue) and the model used in this study (green) (*Hasegawa et al.*, 2011). The left panel is for the entire Bay of Fundy and Gulf of Maine region. The right panel is for the Bay of Fundy region.

2.2.1 Bed Shear Stress Parameterization

Bed shear stress in the model developed by *Hasegawa et al.* (2011) is calculated using the quadratic drag law (*Mellor*, 2004). The quadratic drag law is

$$\vec{\tau_0}(x, y, t) = \rho C_D |\vec{U}| \vec{U}, \tag{2.1}$$

where x, y, and t are horizontal coordinates, and time, respectively, ρ is the seawater density, C_D is the drag coefficient, $\vec{U}$ and $|\vec{U}|$ are the instantaneous near-bed current velocity and speed, respectively. In Equation 2.1, C_D is calculated as follows:

$$C_D = \max\left(\frac{\kappa^2}{\ln^2(z/z_0)}, 2.5 \times 10^{-3}\right), \tag{2.2}$$

where max is the maximum value among enclosed quantities, κ is the Von Kármán constant ($\kappa \approx 0.4$), z is the (positive) vertical coordinate (from the seabed) at which the near-bed current velocity is modeled, and z_0 is the roughness parameter. The law of the wall (see Appendix B for derivation) is used to derive the value of $C_D(z)$ when it is a function z. The value of z varies throughout the model domain and is taken at mid-depth of the σ-level closest to the seabed in the vertical. The remainder of the parameters necessary for the calculation of τ_0 are given the following values: ρ = 1024 kg m^{-3} and z_0 = 0.01 m. The

value of z_0 is the default value in POM.

2.3 Critical Erosion Shear Stress Model

A critical erosion shear stress (τ_c) model was chosen to estimate values of τ_c for sediment samples with mean diameter D_{mean}. The theoretical model of *Wiberg and Smith* (1987) was chosen for this estimation (see Appendix A for derivation). The expression derived by *Wiberg and Smith* (1987) for the non-dimensional critical erosion shear stress is

$$\tau_c^\star(D) = \frac{2}{C_c^D \alpha} \frac{1}{< f^2(z/z_0) >} \frac{\tan\phi_0 \cos\beta - \sin\beta}{1 + (F_c^L/F_c^D)\tan\phi_0}, \tag{2.3}$$

where α is a grain geometry parameter, $< f^2(z/z_0) >$ is the depth-averaged near-bed velocity structure function squared, ϕ_0 is the grain angle of repose, β is the seabed inclination, C_c^D is the critical drag coefficient, F_c^L and F_c^D are the critical lift and drag forces, respectively (see Appendix A for definition of last three variables). Table 2.2 lists the parameter values that are used throughout this study for the calculation of $\tau_c^\star$ and τ_c. $\tau_c^\star$ values are converted to τ_c values by rearranging the equation for the dimensionless critical shear stress: $\tau_c^\star = \tau_c/[(\rho_s - \rho)gD]$. The near-bed velocity profile depends on the flow regime, which for example is $f(z/z_0) = (1/\kappa)\ln(z/z_0)$ for bed roughness Reynolds numbers $R_\star > 100$ ($R_\star = u_\star D/\nu$, where $u_\star$ is the shear velocity). Here, $R_\star$ is based on k_s and the roughness parameter $z_0 = k_s/30$. In other flow regimes, i.e. $R_\star < 100$, $< f(z/z_0) >$ and z_0 have a different functional form and value, respectively. A MATLAB™ script, which was written by Dr. Paul S. Hill, Dalhousie University, was used to calculate values of τ_c. Because $\tau_c^\star$ and $R_c^\star$ depend on τ_c, an initial guess for τ_c is necessary, and the script solves for τ_c by iteration.

2.4 Bilinear Interpolation

Bilinear interpolation was chosen for interpolation of data in this thesis. Bilinear interpolation's main assumption is that a variable's rate of change is linear between data locations. Bilinear interpolation at location (x_k,y_k) to estimate $\hat{Z}$ requires 4 neighboring data (*Glover et al.*, 2011). Figure 2.5 shows the location of these points, which form a rectangle for

Table 2.2: Value of parameters used throughout this study for the calculation of $\tau_c^\star$ and τ_c from *Wiberg and Smith* (1987).

Parameter	Value
β	0 °
α	1.5
ρ	1024 kg m^{-3}
ρ_s	2650 kg m^{-3}
k_s	D_{mean}
D	D_{mean}
ν	$\sim 10^{-6}$ m^2 s^{-1}
ϕ_0	$\sim$ 60 °

simplicity of the example here. The interpolated value $\hat{Z}_k$ is

$$\hat{Z}_k = (1-r_x)(1-r_y)Z_{i,j} + r_x(1-r_y)Z_{i+1,j} + (1-r_x)r_yZ_{i+j+1} + r_xr_yZ_{i+1,j+1} \quad (2.4)$$

where $r_x = (x_k - x_{i,j})/(x_{i+1,j} - x_i, j)$ and $r_y = (y_k - y_{i,j})/(y_{i,j+1} - y_{i,j})$ are fractional distances for a randomly chosen location ($x_{i,j}$,$y_{i,j}$). Bilinear interpolation is often used for estimation with gridded data. Smoothing was also used for map production in this thesis. When sediment samples are heterogeneous both in sampling periods, and methods of collection and analysis, smoothing can help produce better map visual quality. This is the case for the sediment sample data set of this study. The smoothing consists in averaging each map cell with the 8 surrounding cells.

Other interpolation techniques have been tried before bilinear interpolation was chosen. For instance, *Veinot* (2010)produced maps of some of dataset's textural parameters using an optimal interpolation (OI) MATLAB^{TM} script provided by Dr. Keith R. Thompson, Dalhousie University. To estimate a function's value, OI mainly consists in a weighted sum of neighboring data, and can provide an estimate error. The estimate error is an advantage of OI over methods such as bilinear interpolation, which can not provide such an error (*Goff et al.*, 2008). Non-physical results were obtained with OI for several parameters, e.g. negative values were obtained for sorting. Ordinary kriging, a method mathematically similar to OI (*Glover et al.*, 2011), is known to sometimes produce non-physical results (*Deutsch*, 1996). By comparing an interpolated field with individual data, one can assess qualitatively the performance of a technique. Figure 2.6 shows an example

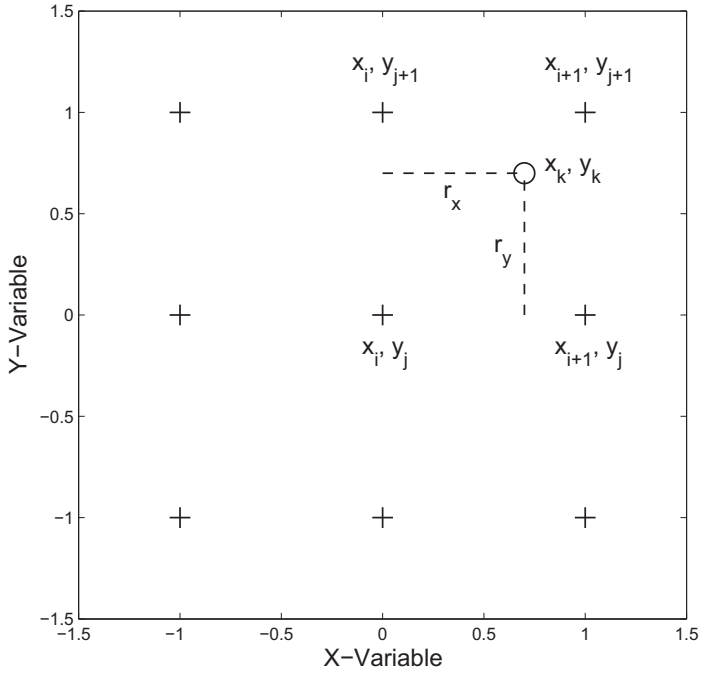

Figure 2.5: Schematic of surrounding data needed for bilinear interpolation of $\hat{Z}_k$ at location (x_k,y_k) (*Glover et al.*, 2011).

of this comparison for mean phi size. This was done for maps produced with bilinear interpolation in this thesis, and the technique proved to be reliable.

Figure 2.6 *(following page)*: An example with mean phi size of comparison between a) samples, b) the interpolated field using bilinear interpolation, and c) the interpolated and smoothed field.

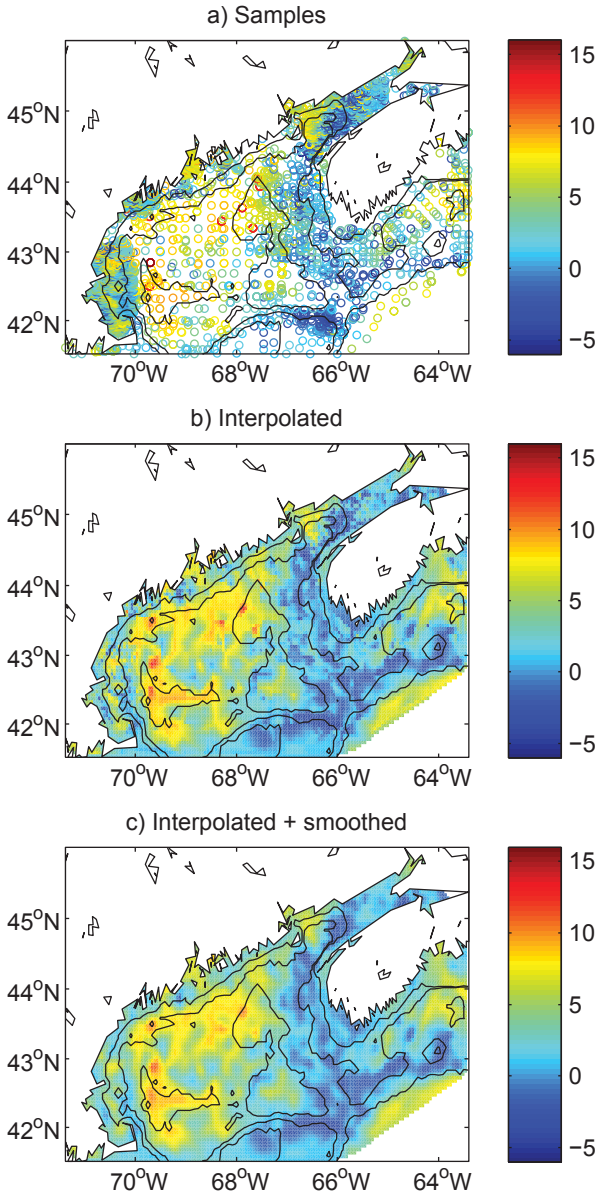
a) Samples
b) Interpolated
c) Interpolated + smoothed
45°N
44°N
43°N
42°N
70°W
68°W
66°W
64°W
15
10
5
0
−5

CHAPTER 3

RESULTS

3.1 Modeled Bed Shear Stress and Observed Sediment Texture

3.1.1 Bed Shear Stress and Near-Bed Velocity

Figures 3.1a and b show maps of maximum modeled tidal bed shear stress and speed 1 m above the seabed in the Bay of Fundy and Gulf of Maine for the $\sim$ 30 d simulation period. Modeled current speeds 1 m above the seabed were calculated with the law of the wall. Maximum bed shear stress is used because it is assumed that maximum near-bed hydrodynamic conditions have a lasting effect on seabed sediment texture. Maximum bed shear stress and its associated velocity 1 m above the seabed are also used by *Signell et al.* (2000) and *Uncles* (1983) to examine the relationship between near-bed hydrodynamics and seabed sediment texture. In general, the Bay of Fundy exhibits higher maximum tidal bed shear stresses (Figure 3.1a) and tidal near-bed current speeds (Figure 3.1b) than the Gulf of Maine. In the Bay of Fundy, the highest maximum tidal bed shear stresses are $\sim$ 40 Pa and associated current speeds 1 m above the seabed are $\sim$ 3 m s^{-1}, and can be found in the Minas Passage. Conversely, the lowest maximum tidal bed shear stresses are $\sim 10^{-2}$ Pa and associated near-bed current speeds are $\sim 10^{-2}$ m s^{-1}, and can be found in coastal regions of the Bay of Fundy ($H <\sim$ 25 m) and the Gulf of Maine ($H <\sim$ 50 m).

Figure 3.2 is map of the modeled tidal range in the Bay of Fundy and Gulf of Maine. Generally, higher ranges in the Bay of Fundy are associated with larger maximum modeled bed shear stresses; and lower ranges are associated with lower maximum bed shear stresses in the basins of the Gulf of Maine and offshore of Maine (Figure 3.1a). In some areas

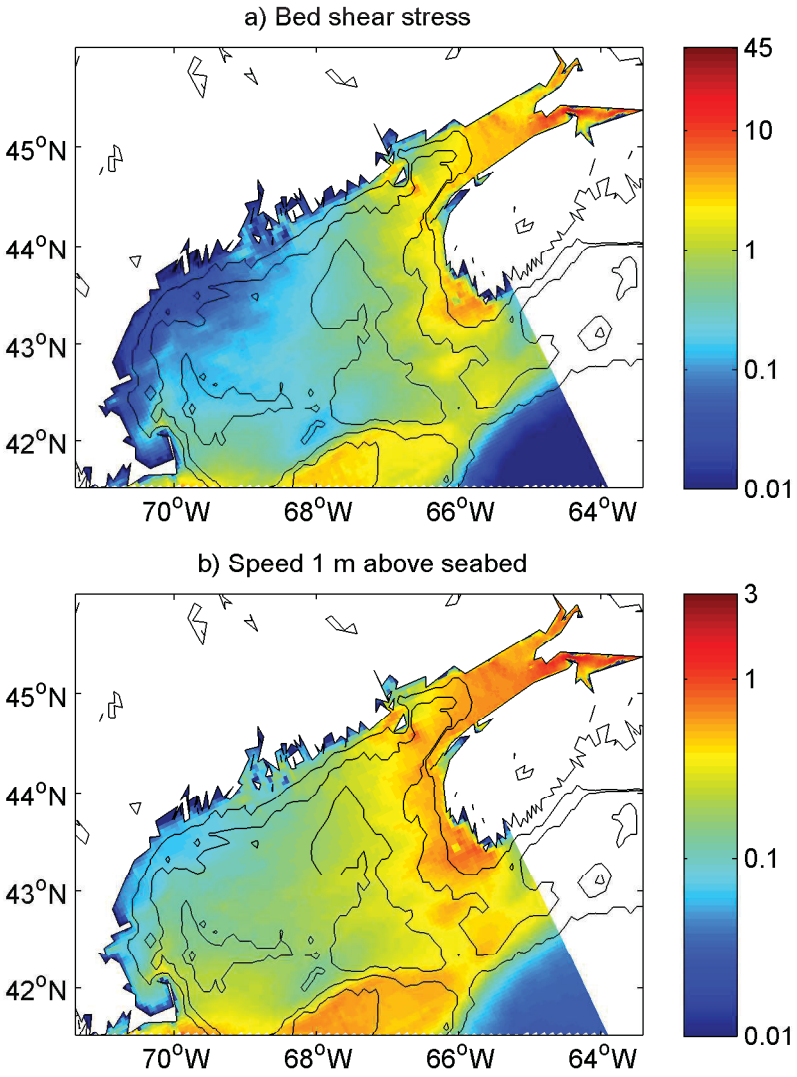

Figure 3.1: a) Map of maximum modeled tidal bed shear stress (in Pa) and b) associated current speed 1 m above the seabed (in m s^{-1}) for the Bay of Fundy and Gulf of Maine region for the simulation $\sim$ 30 d period. This period includes a spring-neap tidal cycle.

where flow is constrained by bathymetry, e.g. Georges Bank, fast tidal flows occur despite lower tidal ranges. The maximum range is $\sim$ 16 m and is found in the Minas Basin.

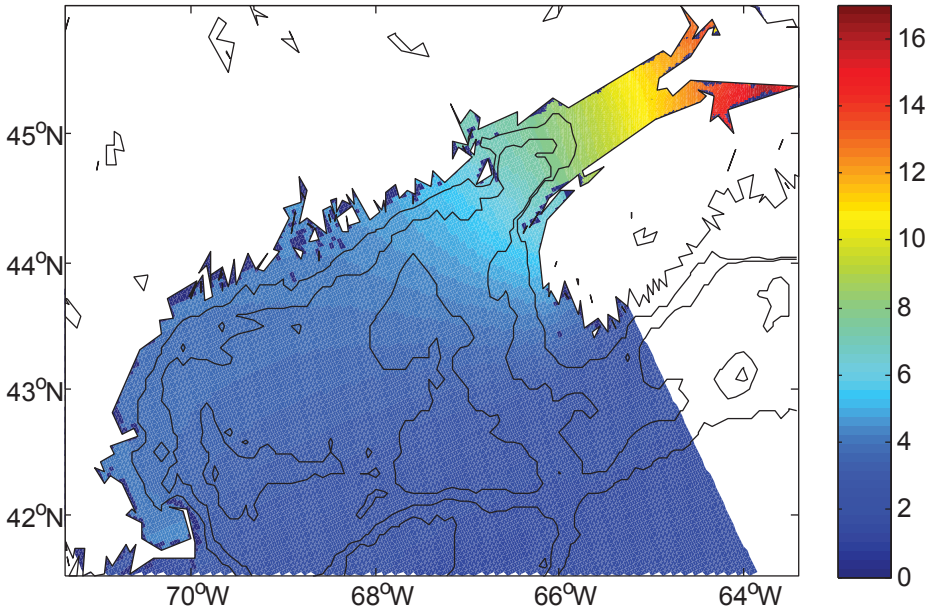

Figure 3.2: Map of modeled tidal range (in m) for the Bay of Fundy and Gulf of Maine region. Macro-tidal environments are those for which the range is $>$ 4 m (*Porter-Smith et al.*, 2004).

3.1.2 Bed Shear Stress and Mean Phi Size

In the Bay of Fundy and Gulf of Maine, larger and smaller mean phi sizes (Figure 3.3a) generally correspond to smaller and larger maximum tidal bed shear stresses (Figure 3.1a), respectively. Recall that larger phi sizes are associated with finer sediments. In the eastern Gulf of Maine (up to the south of Grand Manan Island), Georges Bank, Browns Bank and on the Scotian Shelf, larger maximum tidal bed shear stresses ($>\sim$ 1 Pa) correspond to regions of coarser sediments ($<$ 2 ϕ). In a small number of coastal areas such as on Stellwagen Bank and offshore of Maine's coast, small regions of larger maximum tidal bed shear stress correspond to regions of coarser sediments than surrounding finer sediments. Conversely, in regions of lower maximum tidal bed shear stresses, more specifically offshore of Maine's coast, in the basins of the Gulf of Maine ($H >$ 100 m), the Scotian

Slope and east of Grand Manan Island, finer sediments can be observed. In a transition zone in the northeastern Gulf of Maine (southwest of Grand Manan Island), along Maine's coast and east-southeast of Grand Manan Island, finer sediments are not associated with a decrease in maximum tidal bed shear stresses. There are also a few locations in the Gulf of Maine for which a sharp coarsening in sediments ($\sim$ 2 ϕ) is associated with generally lower maximum tidal bed shear stresses ($\sim$ 1 Pa).

In the Bay of Fundy, which generally has maximum tidal bed shear stresses between $\sim$ 5–10 Pa, except for the Minas Passage, mean phi sizes show variability (between $\sim$ (-2)–6 ϕ). At the mouth of the Avon River, finer mean phi sizes (around $\sim$ 5 ϕ) are associated with lower maximum tidal bed shear stresses ($<\sim$ 1 Pa). In contrast, finer sediments ($\sim$ 2 ϕ) characterize Chignecto Bay also, but these are associated with higher maximum tidal bed shear stresses. In the eastern lower Bay of Fundy, coarser sediments are generally associated with higher maximum tidal bed shear stresses, but patches of finer sediments ($\sim$ 3 ϕ) that are not associated with decreases in maximum bed shear stress are also present.

Figures 3.3b and c comprise scatter, box and density plots that compare maximum modeled bed shear stress and mean phi size for the Gulf of Maine and the Bay of Fundy, respectively. For plots of Figures 3.3b and c, maximum modeled tidal bed shear stress was interpolated with bilinear interpolation to sediment samples' locations. This was also done for scatterplots of other textural parameters in the present section. Competent mean grain size is the largest grain size a flow can set in motion. In scatterplots of Figures 3.3b and c, competent mean phi sizes have been estimated with the critical erosion shear stress τ_c model of *Wiberg and Smith* (1987) and added as curves. This enables a comparison of the competence of modeled flow with observations on a regional scale. For scatterplots

---

Figure 3.3 *(following page)*: a) Map of observed mean phi size in the Bay of Fundy and Gulf of Maine region. The observations were interpolated with bilinear interpolation on a grid with 0.05 ° node-spacing, and were then smoothed with eight surrounding nodes. b) From left to right: scatter, box and density plots of modeled maximum tidal bed shear stress, interpolated at sediment samples' locations, versus mean phi size for the Gulf of Maine. c) Same description as for b), but for the Bay of Fundy. The curves in scatter and density plots represent the competent mean phi sizes estimated with the τ_c model from *Wiberg and Smith* (1987). For boxplots, the boxes' upper and lower edges represent the first and third quartiles, respectively, and the boxes' middle lines represent the medians. The whiskers represent the lowest and highest values within 1.5 times the respective interquartile distances. Crosses represent outliers.

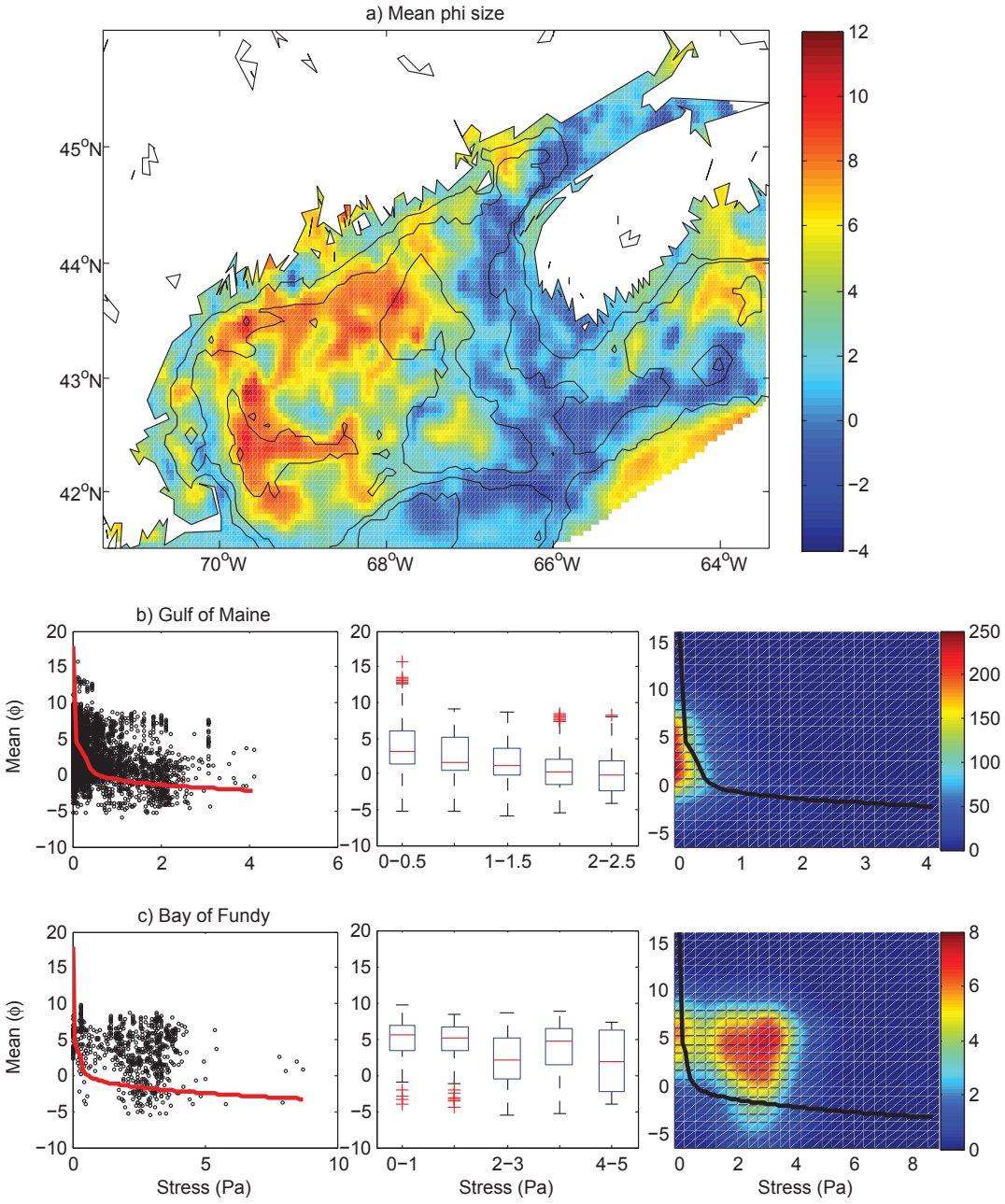
a) Mean phi size
45°N
44°N
43°N
42°N
70°W
68°W
66°W
64°W
12
10
8
6
4
2
0
−2
−4
b) Gulf of Maine
Mean (ϕ)
0–0.5
1–1.5
2–2.5
250
200
150
100
50
0
c) Bay of Fundy
Mean (ϕ)
Stress (Pa)
0–1
2–3
4–5
Stress (Pa)
Stress (Pa)
8
6
4
2
0

of Figures 3.3b and c, mean phi size data was binned in 0.5 and 1 Pa intervals for the Gulf of Maine and Bay of Fundy, respectively. Different bin sizes were chosen for ease of comparison between the two regions. For the Gulf of Maine and the Bay of Fundy, any bin that contained < 1 % and < 2 % of mean phi size data, respectively, was discarded from the analysis. This was also done for scatterplots of other textural parameters in the present section. Discarding bins with few data enables identification of trends in data that are representative of the bulk of data.

For the Gulf of Maine, the scatter and density plot in Figure 3.3b show observed mean phi sizes that are roughly similar to modeled competent mean phi sizes (curves in scatterplot and boxplot). The boxplot in Figure 3.3b shows a decrease in mean phi size medians (an increase in mean grain size median) with increasing maximum modeled tidal bed shear stress. It also shows that mean phi size variability decreases as maximum tidal bed shear stress increases.

For the Bay of Fundy, observed mean phi sizes are generally finer than modeled competent mean phi sizes in Figure 3.3c (curves in scatterplot and boxplot). In the boxplot of Figure 3.3c, mean phi size medians do not show as clear a decrease with increasing maximum tidal bed shear stress as in the Gulf of Maine.

3.1.3 Bed Shear Stress and Gravel Content

Figure 3.4a shows a map of gravel content in the Bay of Fundy and Gulf of Maine region. In the Gulf of Maine, observed gravel content is higher (> 40 %) on the Scotian Shelf, the western Gulf of Maine and the northeastern side of Georges Bank, and is associated with larger maximum modeled tidal bed shear stresses (Figure 3.4a). Higher gravel content (40–60 %) is also found in regions of smaller maximum bed shear stresses, namely north of Cape Cod Bay, in a few locations along Maine's coast and in the shallower parts of the central Gulf of Maine ($100 < H < 200$ m). On the other hand, gravel content is low in the remainder of the Gulf of Maine and east of Grand Manan Island, and is associated with lower maximum bed shear stresses. The larger maximum modeled tidal bed shear stresses in the Bay of Fundy are associated with a range of observed gravel contents. Regions with higher gravel contents are the western lower Bay of Fundy, and some parts of the Minas Basin and Channel. Regions with smaller gravel contents are the eastern lower Bay of Fundy, Chignecto Bay and the mouth of the Avon River, in the Minas Basin.

In the boxplot of Figure 3.4b, gravel content medians increase with increasing maximum

modeled tidal bed shear stress in the Gulf of Maine. For the Bay of Fundy, the boxplot of Figure 3.4c shows gravel content medians are highest for maximum tidal bed shear stresses between 2-3 and 4-5 Pa.

3.1.4 Bed Shear Stress and Sand Content

Figure 3.5a shows a map of sand content in the Bay of Fundy and Gulf of Maine region. In the Gulf of Maine, higher observed sand content (> 40 %) is associated with higher maximum modeled tidal bed shear stresses ($>\sim 1$ Pa), namely on Georges Bank, Stellwagen Bank, the Scotian Shelf, the eastern Gulf of Maine, and along most of Maine's and Cape Cod Bay's coasts (Figure 3.5a). Higher sand content is also found in regions of lower maximum bed shear stresses such as in some of the shallower regions of the Gulf of Maine, and along Maine's coast. On the other hand, regions of low sand content are generally associated with lower maximum bed shear stresses. These regions include the basins of Gulf of Maine, the Scotian Slope, Penobscot Bay, and east of Grand Manan Island. In the Bay of Fundy, higher observed sand content is found in the eastern lower Bay of Fundy, the Minas Channel and Basin, and is associated with higher maximum modeled tidal bed shear stresses (> 5 Pa). Lower sand content is found in the western lower Bay of Fundy and in Chignecto Bay, and is associated with similar maximum bed shear stresses as in higher sand content regions. At the mouth of Chignecto Bay and in a few locations of the western lower Bay of Fundy, regions of higher sand content (between 60–90 %) are also present.

Boxplots in Figure 3.5b show that generally lower sand content medians tend to be associated with higher maximum tidal bed shear stresses in the Gulf of Maine. On the other hand, Figure 3.5c shows that for the Bay of Fundy, the highest sand content median is associated with maximum tidal bed shear stresses between 2-3 Pa.

Figure 3.4 *(following page)*: a) Map of observed gravel content (in % of sample) in the Bay of Fundy and Gulf of Maine region. The observations were interpolated with bilinear interpolation on a grid with 0.05 ° node-spacing, and were then smoothed with eight surrounding nodes. b) From left to right: scatter, box and density plots of modeled maximum tidal bed shear stress, interpolated at sediment samples' locations, versus gravel content for the Gulf of Maine. c) Same description as for b), but for the Bay of Fundy. For boxplots, the boxes' upper and lower edges represent the first and third quartiles, respectively, and the boxes' middle lines represent the medians. The whiskers represent the lowest and highest values within 1.5 times the respective interquartile distances. Crosses represent outliers.

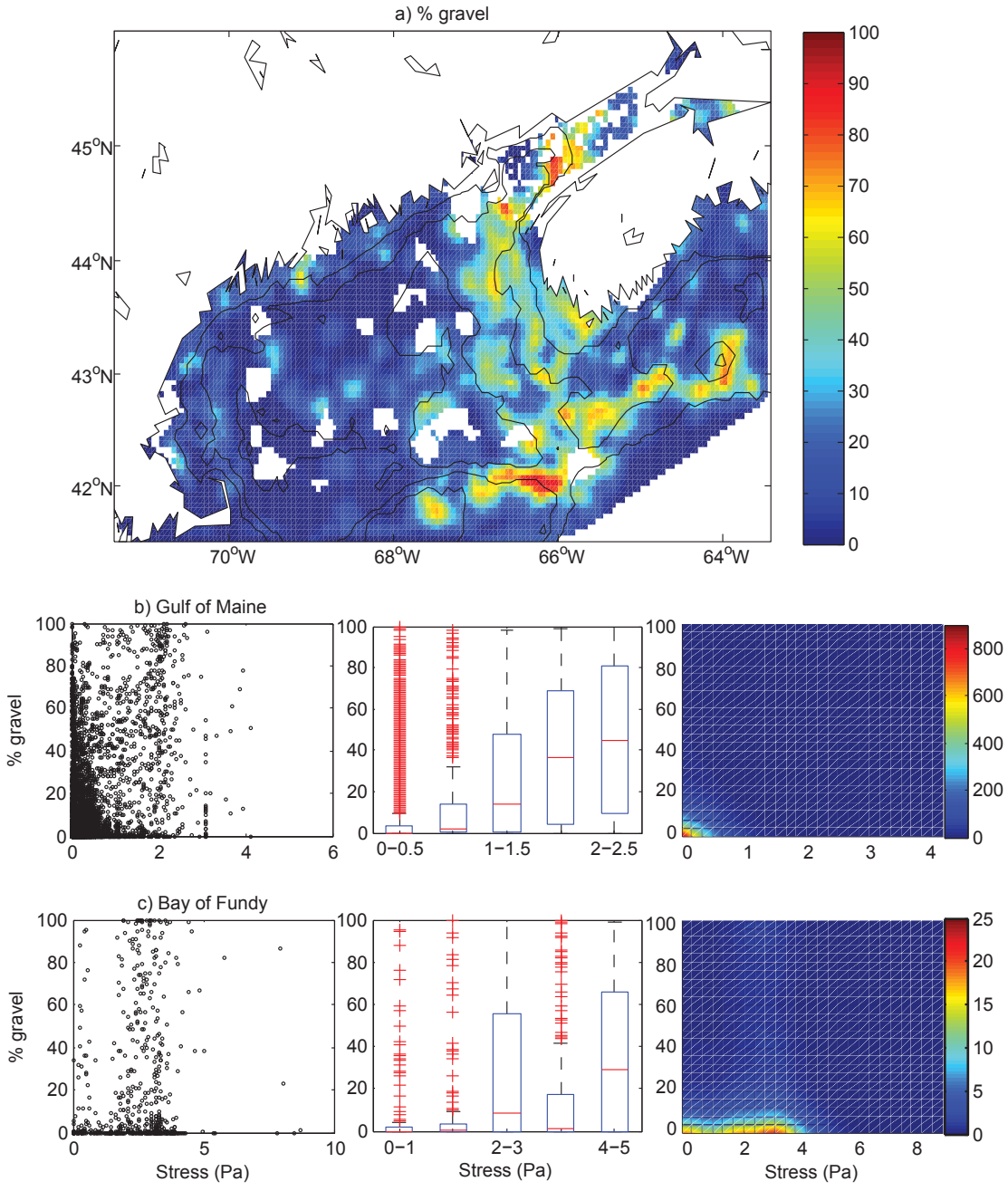
a) % gravel
45°N
44°N
43°N
42°N
70°W
68°W
66°W
64°W
b) Gulf of Maine
% gravel
0–0.5
1–1.5
2–2.5
c) Bay of Fundy
% gravel
0–1
2–3
4–5
Stress (Pa)
Stress (Pa)
Stress (Pa)

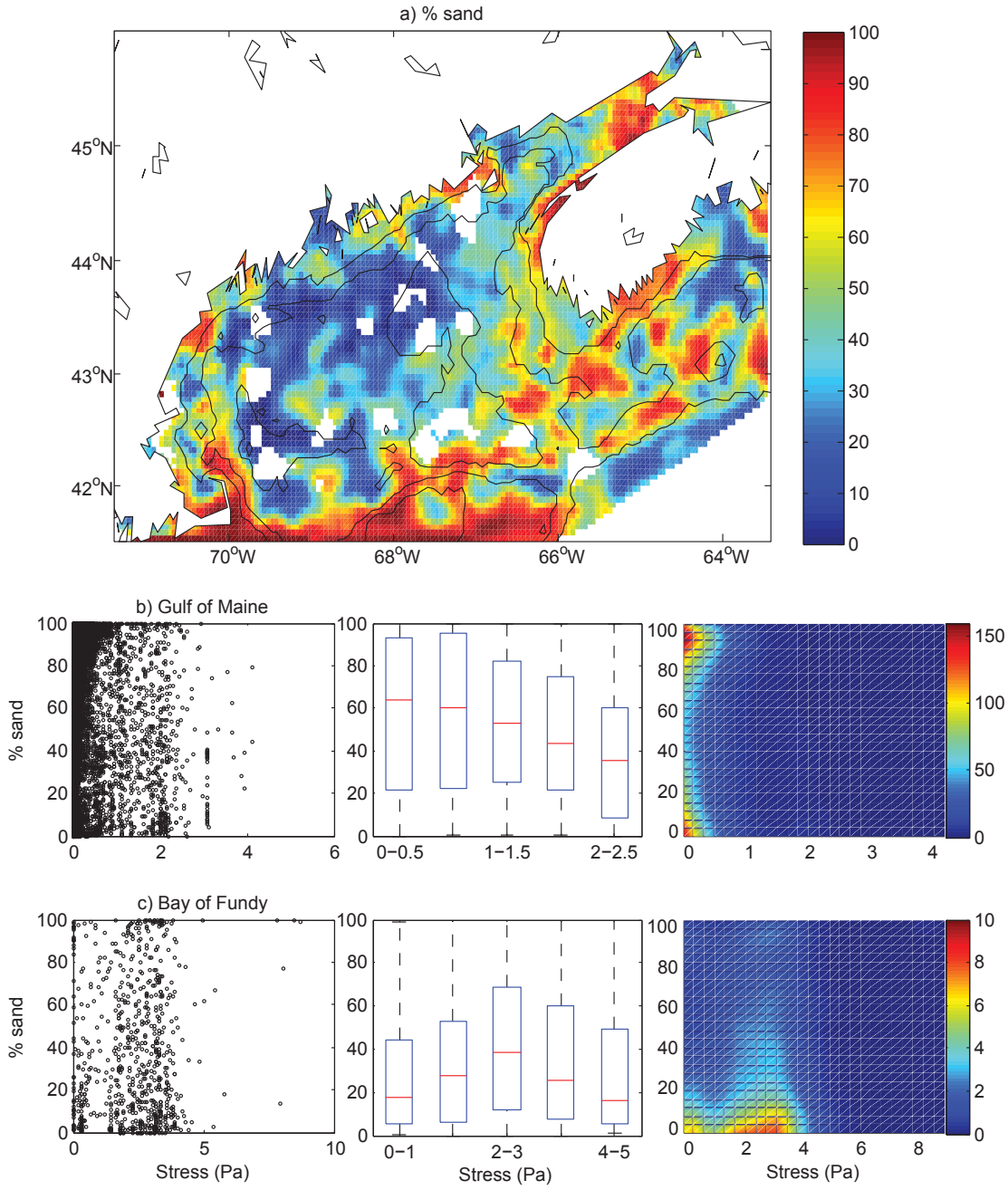

Figure 3.5: Same description as for Figure 3.4, but with observed sand content instead of gravel content.

3.1.5 Bed Shear Stress and Silt and Clay Content

Figure 3.6a shows a map of silt content in the Bay of Fundy and Gulf of Maine region. Larger observed silt contents $> 30\ \%$ (Figure 3.6a) are generally associated with smaller maximum modeled tidal bed shear stresses < 0.5 Pa (Figure 3.1a) in the Bay of Fundy and Gulf of Maine region. Exceptions to this trend are offshore of the coast of Maine, east of Grand Manan Island, in Chignecto bay and in the estuary of the Avon River.

Figure 3.7a shows a map of clay content in the Bay of Fundy and Gulf of Maine region, and patterns with maximum modeled tidal bed shear stress are similar to those observed for silt content. In the Gulf of Maine, observed clay content is highest ($>\sim 30$ %) in the basins of the Gulf of Maine ($H > 50$ m), on the Scotian Slope, along the coast of Maine (> 50 % in Penobscot Bay) and east of Grand Manan Island (Figure 3.7a). These regions are associated with lower maximum modeled tidal bed shear stresses (Figure 3.1a). Higher clay content is also associated with higher maximum bed shear stress in regions such as southeast of Grand Manan Island and south of Murray Basin. On the other hand, lower clay content is associated with higher maximum bed shear stress in regions such as Georges Bank, Stellwagen Bank, the eastern Gulf of Maine and the Scotian Shelf. Lower clay content is also associated with lower maximum bed shear stress along most of the coast of Maine and in some parts of the central Gulf of Maine. The highest observed clay contents of ~ 30 % in the Bay of Fundy are found in upper Chignecto Bay (Figure 3.7a). Clay content is lower in most of the Bay of Fundy (< 5 %), and peaks in clay content (~ 15 %, compared to clay contents $\sim 0\ \%$) are observed in the eastern lower Bay of Fundy and in the estuary of the Avon River, Minas Basin. All low clay contents in the Bay of Fundy are associated with higher maximum modeled tidal bed shear stresses > 5 Pa, except for a region in the estuary of the Avon River.

In the boxplots of Figure 3.6b and Figure 3.7b for the Gulf of Maine, lower silt and clay content medians are associated with higher maximum modeled tidal bed shear stresses. Furthermore, higher silt and clay content variability decreases with increasing maximum bed shear stress in the Gulf of Maine. In the Bay of Fundy, the boxplots of Figure 3.6c and Figure 3.7c show that lowest silt and clay content medians are found at maximum tidal bed shear stresses between 2-3 Pa.

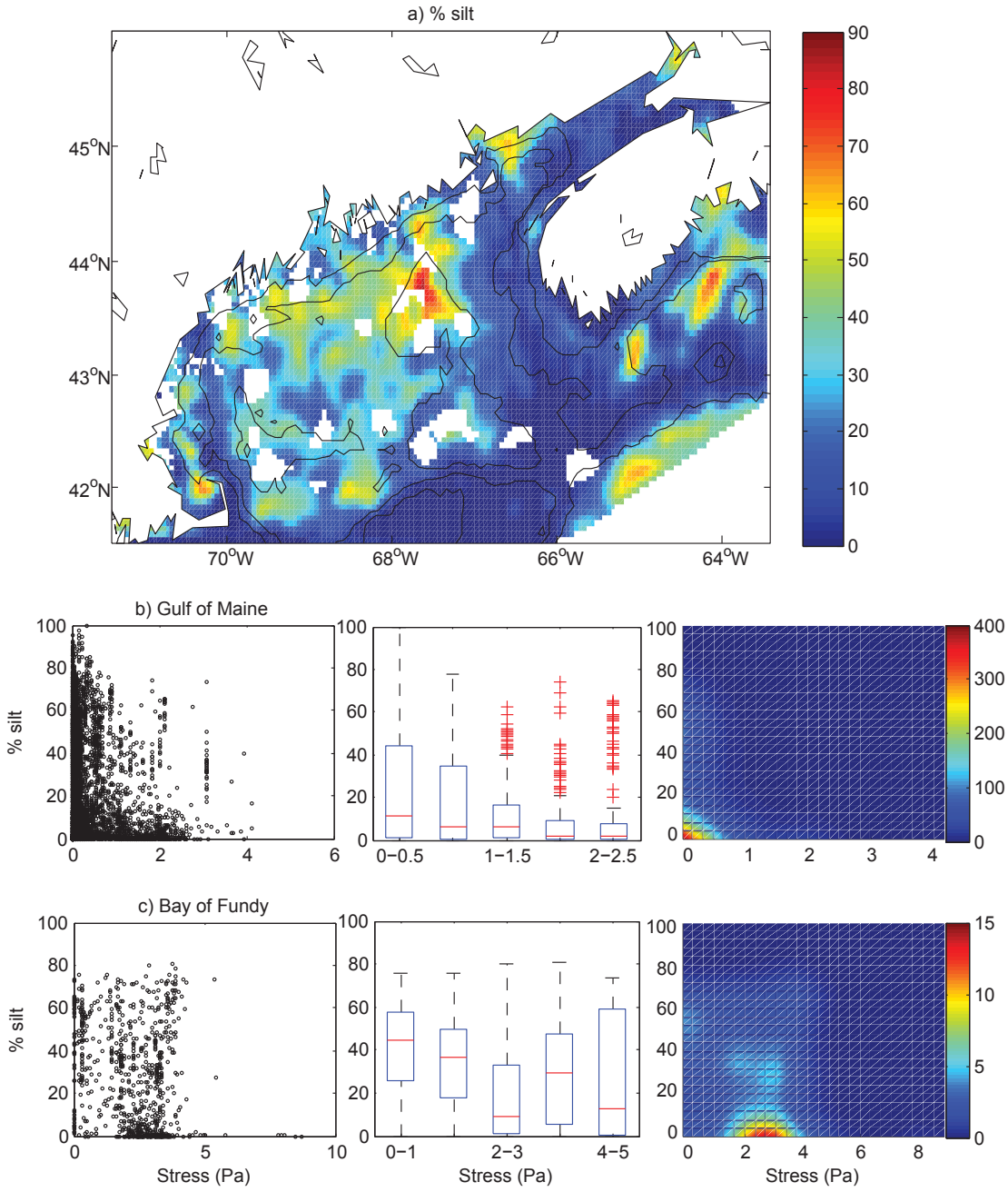

Figure 3.6: Same description as for Figure 3.4, but with observed silt content instead of gravel content.

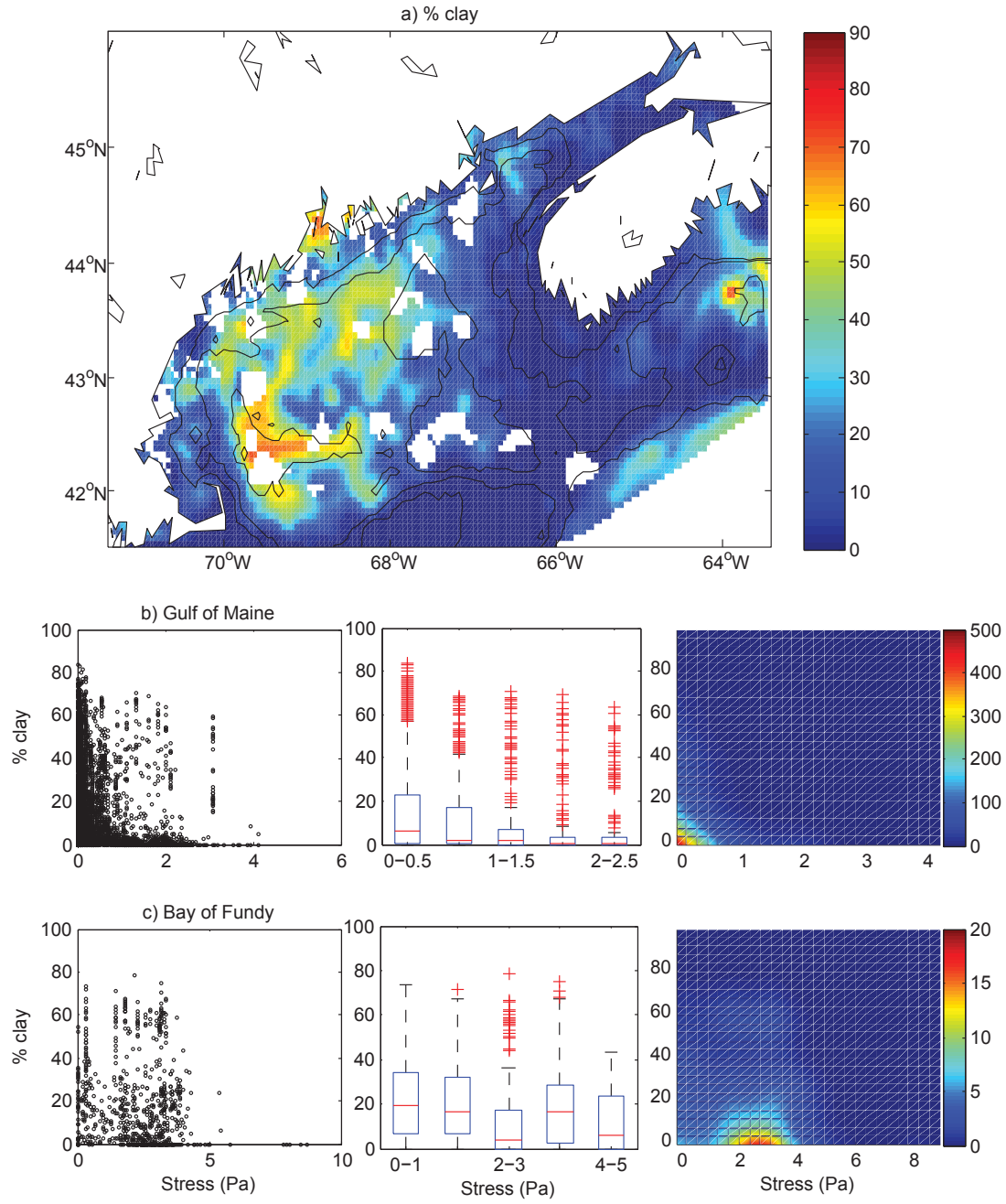

Figure 3.7: Same description as for Figure 3.4, but with observed clay content instead of gravel content.

3.2 Observed and Competent Mean Phi Sizes

3.2.1 All Observed and Competent Mean Phi Sizes

Figure 3.8 shows correlation between observed and competent mean phi sizes. Correlation of observed and competent mean phi sizes provides another means of comparing observations with the model output. Maximum bed shear stress will determine mean grain size under the assumptions that (1) tidal bed shear stresses are the dominant source of bed shear stress, (2) all grain sizes are resuspended at the maximum bed shear stress (*Buffington and Montgomery*, 1999), (3) there is a residual near-bed flow, and (4) sediment supply of grain sizes smaller than competence of near-bed flow does not exceed the transport capacity of near-bed flow. Coefficients of determination R^2 values were calculated for 0.5 ° boxes with 0.25 ° overlap. When R^2 values were based on < 10 sediment samples, these were discarded from the analysis. Figure 3.9 shows the statistical significance of R^2. When $p > 0.05$, R^2 value is not statistically different from 0. The coefficient of determination R^2 between observations O and predictions P is: $R^2 = \left[\sum_{i=1}^{n}(O_i - \bar{O})(P_i - \bar{P})\right]^2 / \left[\sum_{i=1}^{n}(O_i - \bar{O})^2 \sum_{i=1}^{n}(P_i - \bar{P})^2\right]$, where O_i and P_i are the i-th instance of variables O and P, respectively, $\bar{O}$ and $\bar{P}$ are the means of O and P, respectively, and n is the number of observations and predictions. R^2 quantifies how much of the dependent variable's variance is explained by the independent variable's variance using a linear relationship (*Bethea et al.*, 1995).

The correlation between observed and competent mean phi sizes is generally better in the Gulf of Maine than in the Bay of Fundy (Figure 3.8). R^2 values generally between $\sim$ 0.3–0.8 are found on Georges Bank and Basin, the Scotian Slope, in the eastern Gulf of Maine west of the Scotian Shelf, on Stellwagen Bank and in Cape Cod Bay. R^2 values up to 0.5 are calculated for Murray and Jordan Basins in the Gulf of Maine, but smaller values are generally calculated for these basins. The highest R^2 values in the Gulf of Maine are on Georges Bank and the Scotian Slope, and are ~ 0.8. Lower R^2 values are calculated for

---

Figure 3.8 *(following page)*: Map of coefficient of determination (R^2) between observed and competent mean phi sizes for boxes of 0.5 ° with 0.25 ° overlap. For panels, the 1:1 line shows exact agreement between observations and predictions. Average absolute error ϵ_M values are also given for comparison with R^2 values. Competent mean phi sizes are computed using maximum modeled tidal bed shear stress and the expression for critical erosion shear stress of *Wiberg and Smith* (1987).

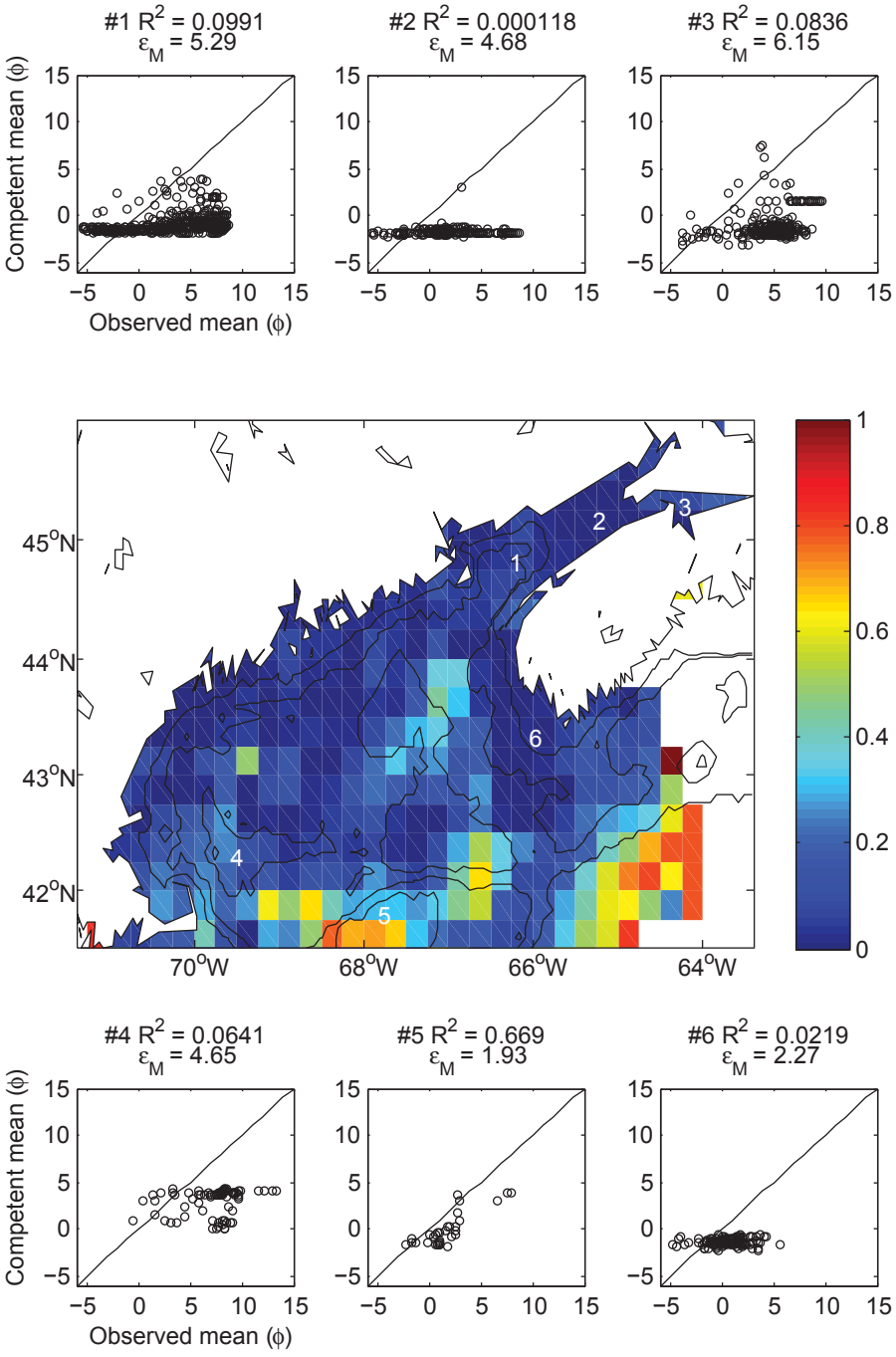
#1 R2 = 0.0991
εM = 5.29
#2 R2 = 0.000118
εM = 4.68
#3 R2 = 0.0836
εM = 6.15
Competent mean (ϕ)
Observed mean (ϕ)
45°N
44°N
43°N
42°N
70°W
68°W
66°W
64°W
1
2
3
4
5
6
#4 R2 = 0.0641
εM = 4.65
#5 R2 = 0.669
εM = 1.93
#6 R2 = 0.0219
εM = 2.27

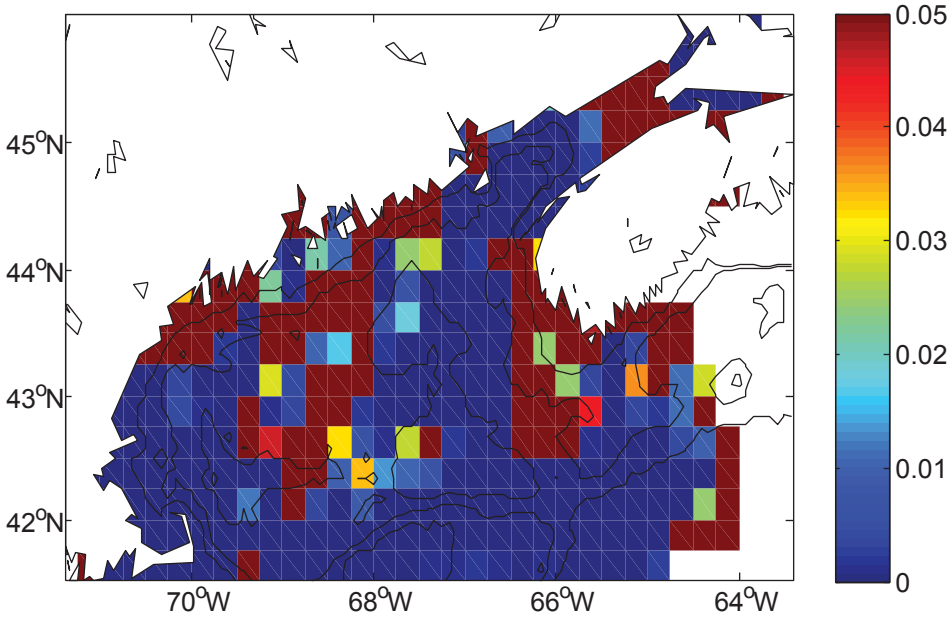

Figure 3.9: Map of p-values for R^2 values in Figure 3.8. When p-value > 0.05 (burgundy boxes), R^2 value is statistically non-significant.

the remainder of the Gulf of Maine and the Bay of Fundy. In the Bay of Fundy, maximum R^2 values are of ~ 0.2. R^2 values are generally higher for the western lower Bay of Fundy, the Minas Channel and Cobequid Bay.

The three upper panels of Figure 3.8 show different relationship types between observed and competent mean phi sizes for the Bay of Fundy. The western lower Bay of Fundy location (box # 1 centered on 44.75 °N and 66.25 °W) shows a majority of competent mean phi sizes that are smaller than observed mean phi sizes (data points below the 1:1 line). Recall that larger phi sizes represent finer sediments. Many competent mean phi sizes, on the other hand, are larger (around -1 ϕ) than observed mean phi sizes (between (-6)–(-2) ϕ). In addition, there is some variability in competent mean phi sizes as well as in observed mean phi sizes. The eastern lower Bay of Fundy location (box # 2 centered on

45.25 °N and 65.25 °W) shows competent mean phi sizes that are larger than observed mean phi sizes, but most competent mean phi sizes are smaller than observed mean phi sizes. Competent mean phi sizes are aggregated around $\sim$ -2 ϕ, and observed mean phi sizes range from (-6)–10 ϕ. In the Minas Basin location (box # 3 centered on 45.5 °N and 64.25 °W), most competent mean phi sizes (up to $\sim$ 8 ϕ) are smaller than observed mean phi sizes. On the other hand, competent mean phi sizes that are larger than observed mean phi sizes lie close to the 1:1 line, which represents exact agreement between predictions and observations. The R^2 value for the eastern lower Bay of Fundy location is statistically non-significant ($p > 0.05$, correlation coefficient R is not statistically different from 0, Figure 3.9).

The three lower panels in Figure 3.8 show different relationship types between observed and competent mean phi sizes for the Gulf of Maine. A high R^2 of 0.67 is calculated for the Georges Bank location (box # 5 centered on 41.75 °N and 67.75 °W,). Competent mean phi sizes tend to be generally smaller than observed mean phi sizes. For the Murray Basin location (box # 4 centered on 42.25 °N and 69.5 °W), most competent mean phi sizes (between 0–5 ϕ) are smaller than observed mean phi sizes (between $\sim$ 0–15 ϕ), and there is good agreement between smallest competent mean phi sizes and smallest observed mean phi sizes. A similar pattern as for the eastern lower Bay of Fundy location is denoted for the the Scotian Shelf location (box # 6 centered on 43.25 °N and 66 °W): most competent mean phi sizes are smaller than observed mean phi sizes, and a few competent mean phi sizes are larger than observed mean phi sizes. The R^2 value for the Scotian Shelf location is statistically non-significant (Figure 3.9).

Figure 3.10 shows mean absolute error ϵ_M values for the Bay of Fundy and Gulf of Maine. For Figure 3.10, mean absolute error ϵ_M values were calculated for the same boxes as for R^2 values in Figure 3.8. The mean absolute error ϵ_M quantifies the average absolute difference between observations and predictions from a model (*Stow et al.*, 2009). ϵ_M is defined for all n in a given box by:

$$\epsilon_M = \frac{1}{n} \sum_{i=1}^{n} |P_i - O_i|, \tag{3.1}$$

where parallel bars denote the absolute value of the enclosed quantity. Note that R^2 and ϵ_M are complementary measures of agreement between observations and predictions. R^2

is a measure of correlation between observed and competent grain sizes. Correlation can be good even if magnitudes do not agree. In contrast, ϵ_M is a measure of agreement in magnitude between observed and competent grain sizes. For a sediment texture in hydrodynamic equilibrium, R^2 between observed and competent mean phi sizes is large, and ϵ_M is small.

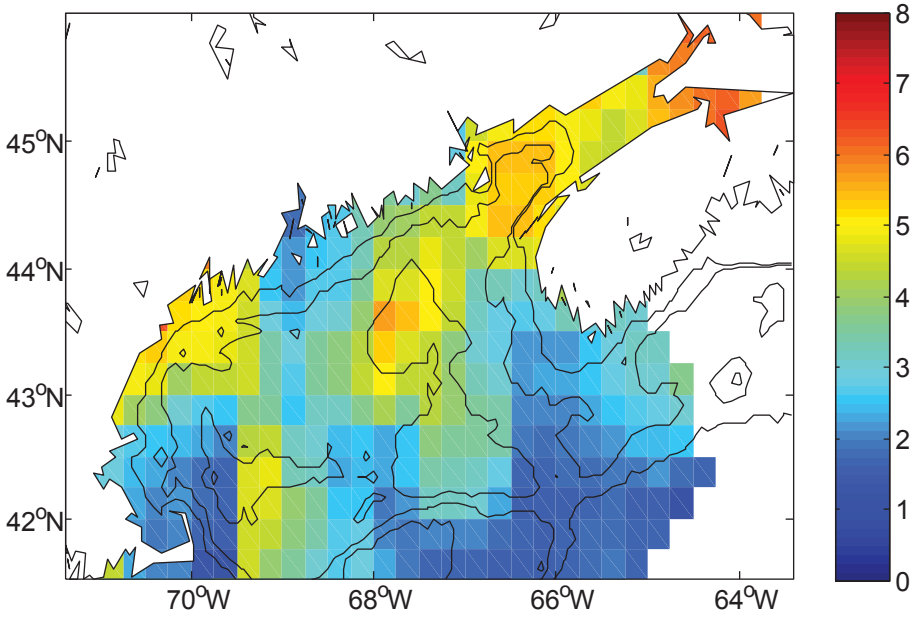

Figure 3.10: Map of mean absolute error ϵ_M values between observed and competent mean phi sizes for boxes of 0.5 ° with 0.25 ° overlap. The boxes are the same as for R^2 values in Figure 3.8.

Figure 3.10 shows that ϵ_M values are generally lower in the Gulf of Maine than in the Bay of Fundy. This means that there is generally better agreement between observed and competent mean phi sizes in the Gulf of Maine. Generally lower ϵ_M values < 3 are calculated offshore of Penobscot Bay, in and around Cap Cod Bay, on Georges Bank and the Scotian Shelf, in the eastern Gulf of Maine and on the Scotian Slope. Generally higher

ϵ_M values are calculated offshore of Maine's coast, in Murray and Jordan Basins, and in all of the Bay of Fundy, with maximum values for the upper Bay of Fundy.

3.2.2 Bin-Averaged Observed and Competent Mean Phi Sizes

Figure 3.11 shows R^2 values between 1-ϕ bin-averaged observed and competent mean phi sizes. Bin-averaging enables a comparison to be made on the basis of a group of samples, instead of on the basis of individual samples. To obtain this figure, the observed and competent mean phi sizes of each box in Figure 3.8 were averaged over 1-ϕ bins and then correlated to obtain R^2 values. The values of ϵ_M in Figure 3.13 were obtained with the same boxes and bin-averaged values as for Figure 3.11.

In Figure 3.11, 1-ϕ bin-averaged R^2 values between observed and competent mean phi sizes are generally higher than non-bin-averaged R^2 values in Figure 3.8. Regions where bin-averaging does not generally yield higher R^2 values, i.e. R^2 values remain < 0.1, are the shallower Scotian Shelf ($H < 100$ m), the northwestern Gulf of Maine and the lower eastern Bay of Fundy. Coastal areas for which R^2 values remain < 0.1 are Penobscot and Passamaquoddy Bays, and the Avon River's estuary. In these areas where bin-averaged R^2 values generally are < 0.1, Figure 3.12 shows that R^2 values are generally statistically non-significant.

The relationship types noted for observed and competent mean phi sizes in panels of Figure 3.8 remain after bin-averaging. In Figure 3.13, bin-averaged ϵ_M values are generally similar to those of non-bin-averaged ϵ_M values (Figure 3.10). Lower ϵ_M values, however, are generally calculated for the entire Bay of Fundy.

3.3 Sediment Transport Proxies

3.3.1 Residual Bed Shear Stress

Figure 3.14 shows residual modeled tidal bed shear stress magnitude for the Bay of Fundy and Gulf of Maine. It was calculated as follows: $\bar{\tau_0} = |1/T_s \int_0^{T_s} \vec{\tau_0} \mathrm{d}t|$, where T_s is the

---

Figure 3.11 *(following page)*: Map of coefficient of determination R^2 between 1-ϕ bin-averaged observed and competent mean phi sizes for boxes of 0.5 ° with 0.25 ° overlap. The boxes are the same as for R^2 values in Figure 3.8. Average absolute error ϵ_M values are also given for comparison with R^2 values. competent mean phi sizes are computed using maximum modeled tidal bed shear stress and the expression for critical erosion shear stress of *Wiberg and Smith* (1987).

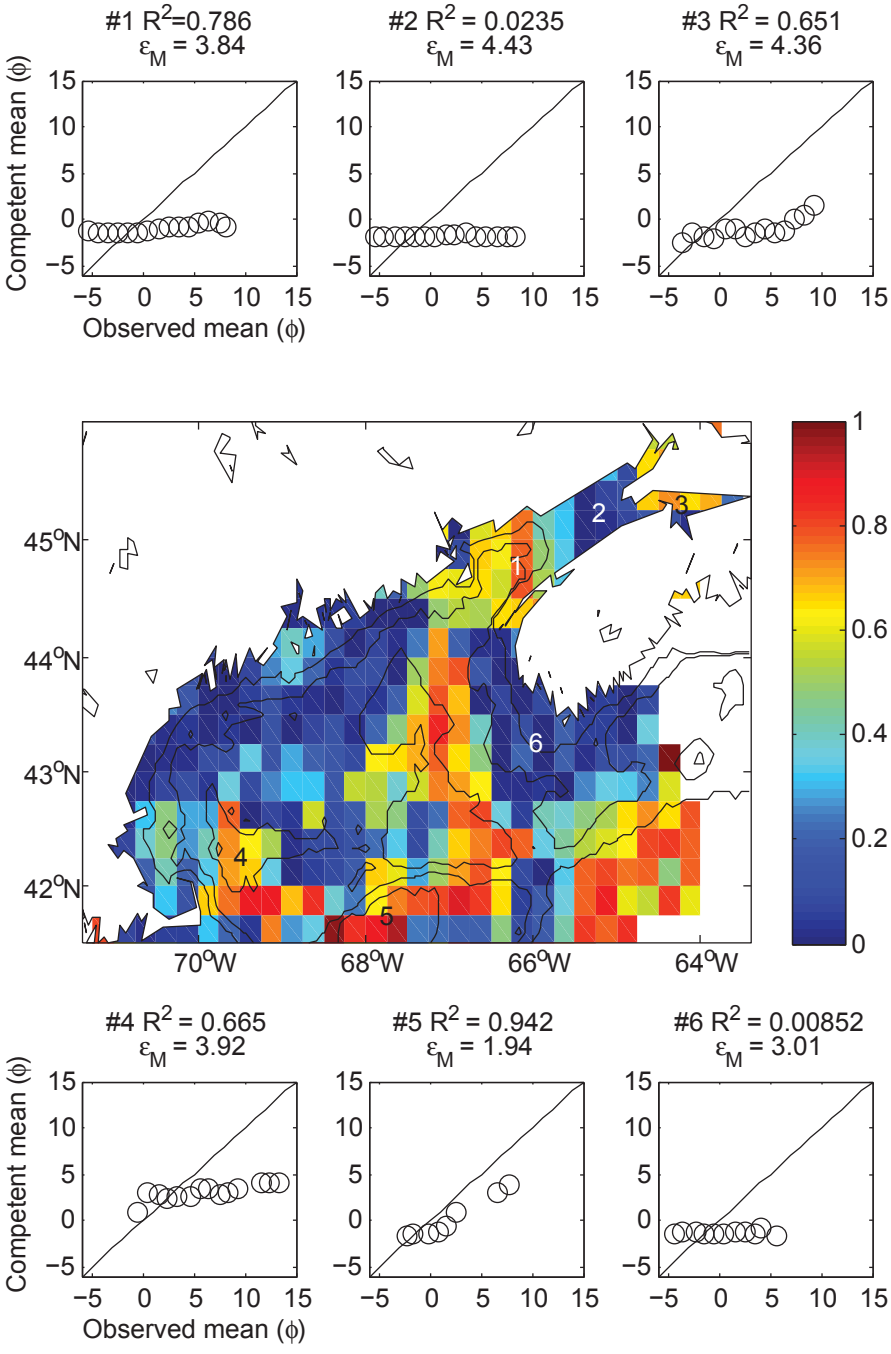
#1 R2=0.786
εM = 3.84
#2 R2 = 0.0235
εM = 4.43
#3 R2 = 0.651
εM = 4.36
Competent mean (ϕ)
Observed mean (ϕ)
45°N
44°N
43°N
42°N
70°W
68°W
66°W
64°W
1
2
3
4
5
6
#4 R2 = 0.665
εM = 3.92
#5 R2 = 0.942
εM = 1.94
#6 R2 = 0.00852
εM = 3.01

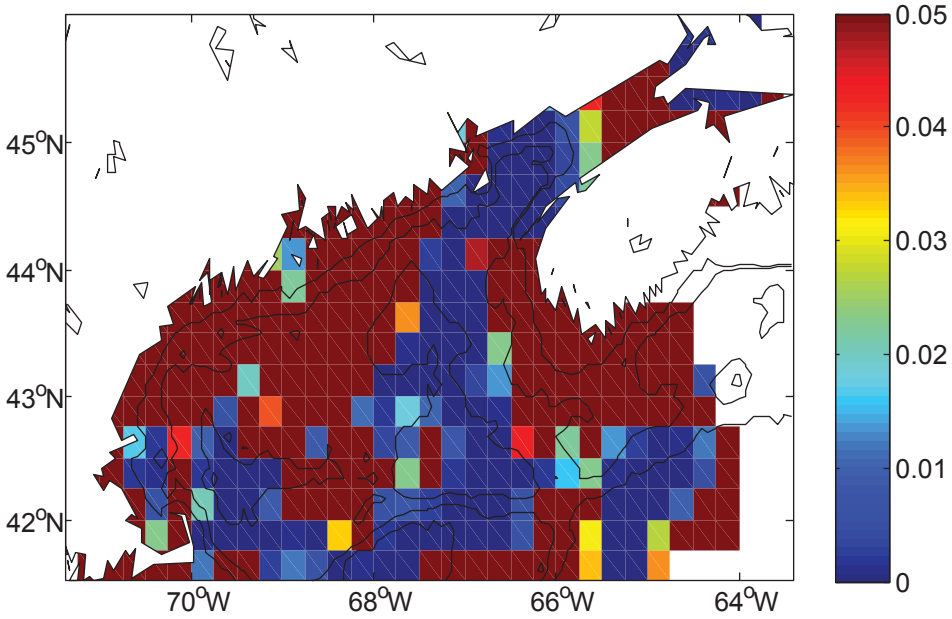

Figure 3.12: Map of p-values for R^2 values in Figure 3.11. When p-value > 0.05 (burgundy boxes), R^2 value is statistically non-significant.

model integration period, and t is time. In the present study, T_s equals the simulation period of $\sim$ 30 d, and $\bar{\tau}_0$ was computed numerically. Larger ($> 10^{-2}$ Pa) values of residual modeled tidal bed shear stress magnitude are in the Bay of Fundy. Residual modeled tidal bed shear stress vectors form a clockwise gyre in the lower western Bay of Fundy, form a counter-clockwise gyre west of the Minas Passage, and a clockwise gyre east of the Minas Passage; these vectors follow isobaths in a clockwise direction on Georges Bank; and they flow southward close to the 100-m isobath off the Scotian Shelf.

3.3.2 Critical Erosion Shear Stress Exceedence

Figure 3.15 shows the % of time the estimated critical erosion shear stress τ_c for a texture class is exceeded by the magnitude of modeled tidal bed shear stresses. This percentage

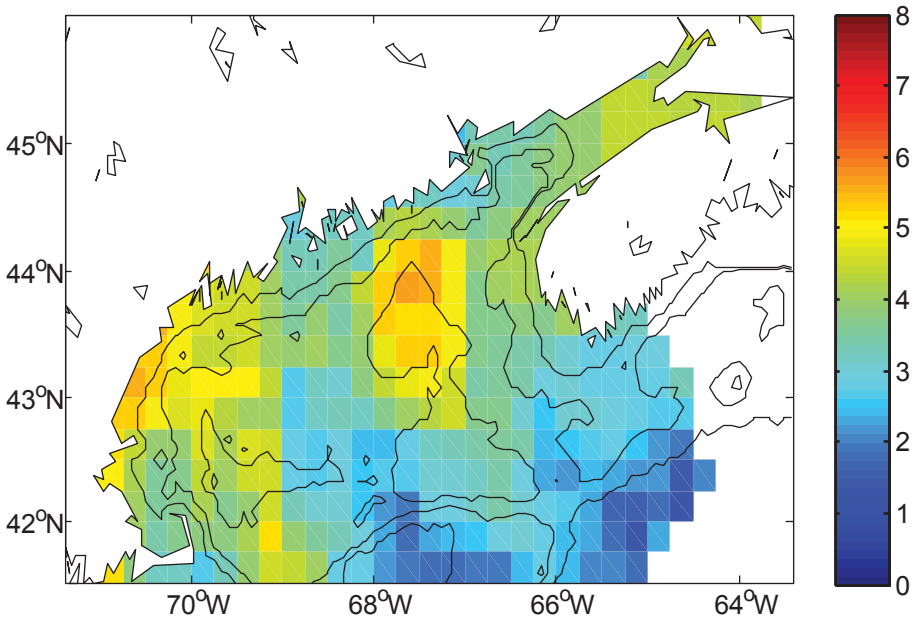

Figure 3.13: Map of mean absolute error ϵ_M values between 1-ϕ bin-averaged observed and competent mean phi sizes for boxes of 0.5 ° with 0.25 ° overlap. The boxes are the same as for R^2 values in Figure 3.8.

was calculated to estimate the frequency to which several texture classes are resuspended. τ_c values are based on the smallest size of textural classes (Table 2.1), and calculated with the expression of *Wiberg and Smith* (1987) for τ_c. The % of time was calculated with respect to the entire simulation period, which is $\sim$ 30 d and includes a spring-neap tidal cycle.

In Figure 3.15, the Bay of Fundy shows that estimated critical erosion shear stresses τ_c for fine silt, sand and gravel, are exceeded by the magnitude of modeled tidal bed shear stresses generally a larger part of the time than in Gulf of Maine. The τ_c value for fine silt is exceeded $>$ 90 % for all of the Bay of the Fundy. Similarly to fine silt, τ_c for fine sand is exceeded between 80–100 % of the time, with maximum values in the Minas Passage,

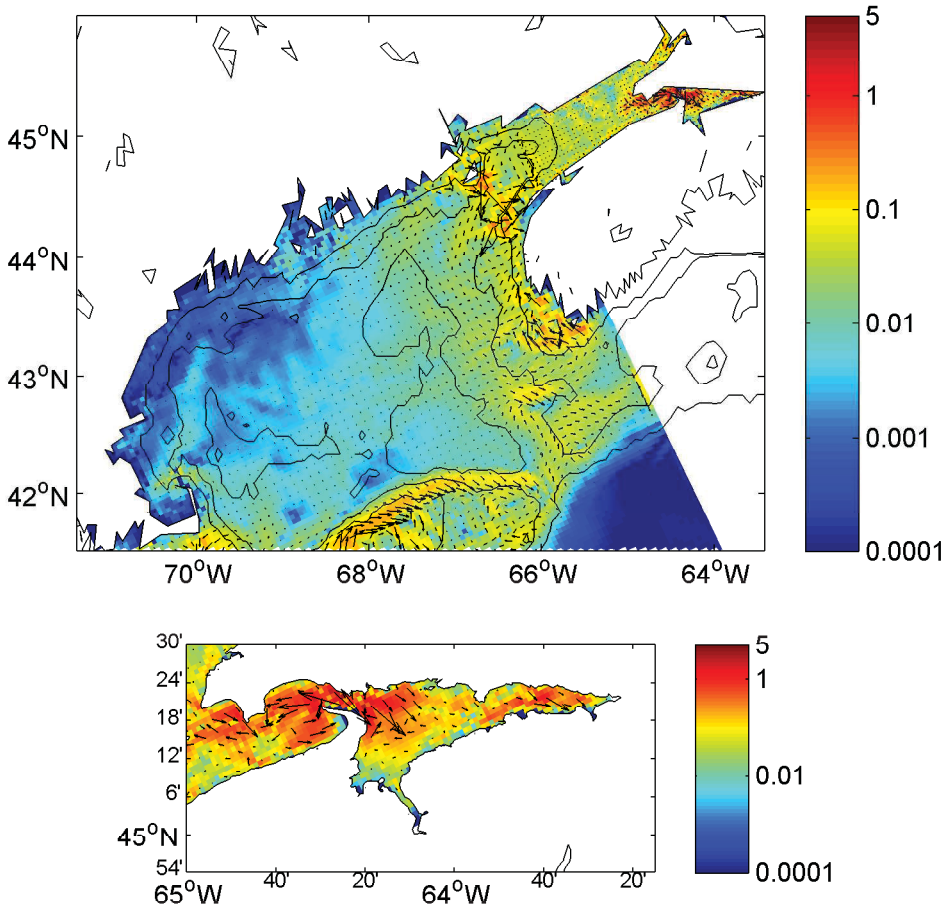

Figure 3.14: Map of residual modeled tidal bed shear stress vectors (arrows, in Pa) and associated magnitude (color, in Pa) for the Bay of Fundy and Gulf of Maine (upper panel) and Minas Basin regions (lower panel). The vectors' length is not indicative of residuals' magnitude, the colorbar quantifies this magnitude. The density of model vectors is reduced by a factor of two in the Gulf of Maine domain, and by a factor of three in the Bay of Fundy domain. The period for the time-averaging is the model simulation period.

Channel and Basin. In the Bay of Fundy, modeled tidal bed shear stress magnitudes exceed the estimated critical erosion shear stress τ_c of fine gravel in a more variable way than the Gulf of Maine, with values between between 0–90 % of the time. More specifically, in the western lower Bay of Fundy, τ_c for fine gravel is exceeded between 0–40 % of the time. These last values are between 0–70 % of the time in the eastern lower Bay of Fundy. The τ_c value for fine gravel is exceeded $\sim$ 90 % of the time in the Minas Channel and Cobequid Bay, in the Minas Basin. These are maximum values for the whole Bay of Fundy and Gulf of Maine region. The τ_c value for fine gravel is exceeded $\sim$ 60 % of the time in the Minas Channel and most of Minas Basin. Exceptions to this are the Southern Bight and Scots Bay, where modeled bed shear stresses almost never exceed τ_c for fine gravel.

Critical erosion shear stress exceedence times of different textural classes vary greatly both among textural classes and spatially in the Gulf of Maine region (Figure 3.15). In the Gulf of Maine, τ_c for 3.9-μm fine silt is exceeded by the magnitude of modeled bed shear stresses most of the time (80–100 %). Exceptions to this are along most of Maine and Cape Cod Bay's coasts, and on the Scotian Slope, where it is almost never exceeded ($\sim$ 0 %). The τ_c value for 62.5-μm fine sand is exceeded by the magnitude of modeled tidal bed shear stresses a 100 % of the time on Georges Bank. Other areas where τ_c for fine sand is exceeded a large part of the time (between 60–90 %) are the Scotian Shelf and the eastern Gulf of Maine. More specifically, τ_c for fine sand is exceeded at most 60 % of the time in the eastern parts of Georges and Jordan Basins, east of Grand Manan Island and in the Northeast Channel. Interestingly, τ_c for fine sand is exceeded at most $\sim$ 80 % of the time on Stellwagen Bank. On the other hand, 2-mm fine gravel is at rest all the time for most of the Gulf Maine, with the magnitude of modeled tidal bed shear stresses rarely rising above its τ_c value. The τ_c value for fine gravel is exceeded 60 % of the time on the Scotian Shelf (mainly at $H < 50$ m), while on the western flank of Georges Bank this reaches 40 % of the time.

Figure 3.15 *(following page)*: Maps of % of the time the estimated critical erosion shear stress τ_c for a) fine silt (D = 3.9 μm), b) fine sand (62.5 μm), and c) fine gravel (2 mm), is exceeded by the magnitude of modeled tidal bed shear stresses. The % of time is over the entire simulation period, which is $\sim$ 30 d.

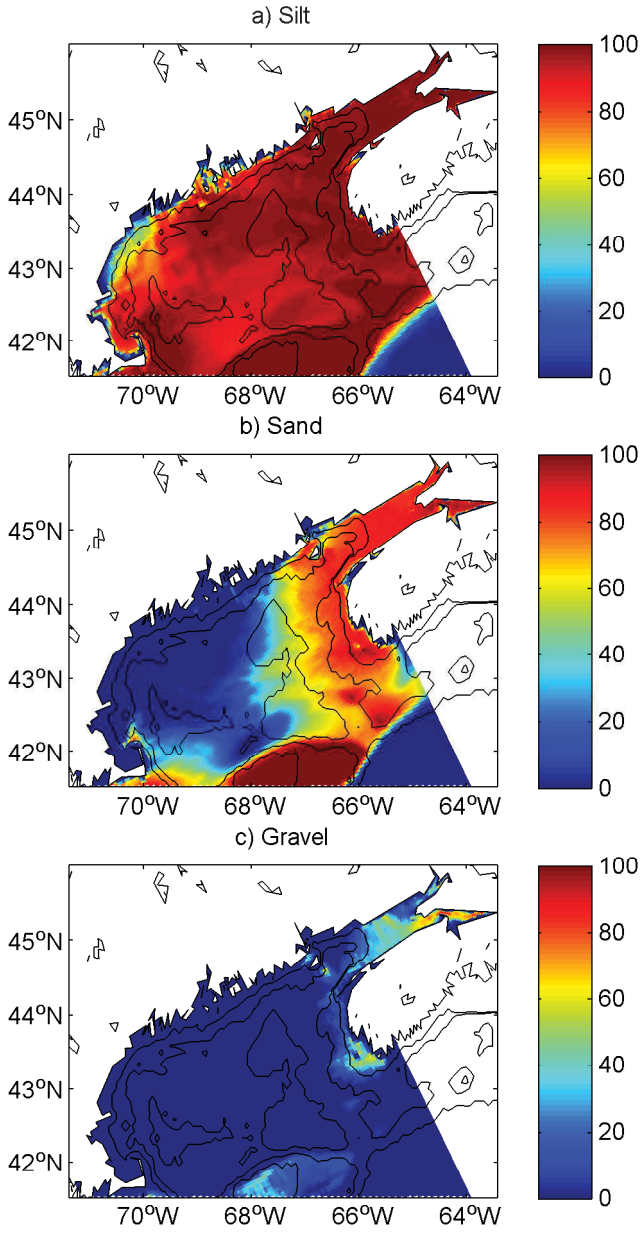
a) Silt
45°N
44°N
43°N
42°N
70°W
68°W
66°W
64°W
100
80
60
40
20
0
b) Sand
45°N
44°N
43°N
42°N
70°W
68°W
66°W
64°W
100
80
60
40
20
0
c) Gravel
45°N
44°N
43°N
42°N
70°W
68°W
66°W
64°W
100
80
60
40
20
0

3.3.3 Sediment Sorting

Figure 3.16a shows a map of sediment sorting for the Bay of Fundy and Gulf of Maine region. In the Gulf of Maine, better sorted sediments ($< 3\ \phi$) are observed on Georges Bank, Stellwagen Bank, Browns Bank, the Scotian Shelf and east of Grand Manan Island. Better sorted sediments also occur in Penobscot Bay, Cape Cod Bay, along most of the coast of the Gulf of Maine and in the major basins of the Gulf of Maine. Sediments that are less sorted are in the shallower parts of the Gulf of Maine ($100 < H < 200$ m) and along the coast of Maine in regions such as offshore of Penobscot Bay. Less sorted sediments are also in the northeastern part of the Gulf of Maine at the mouth of the lower Bay of Fundy.

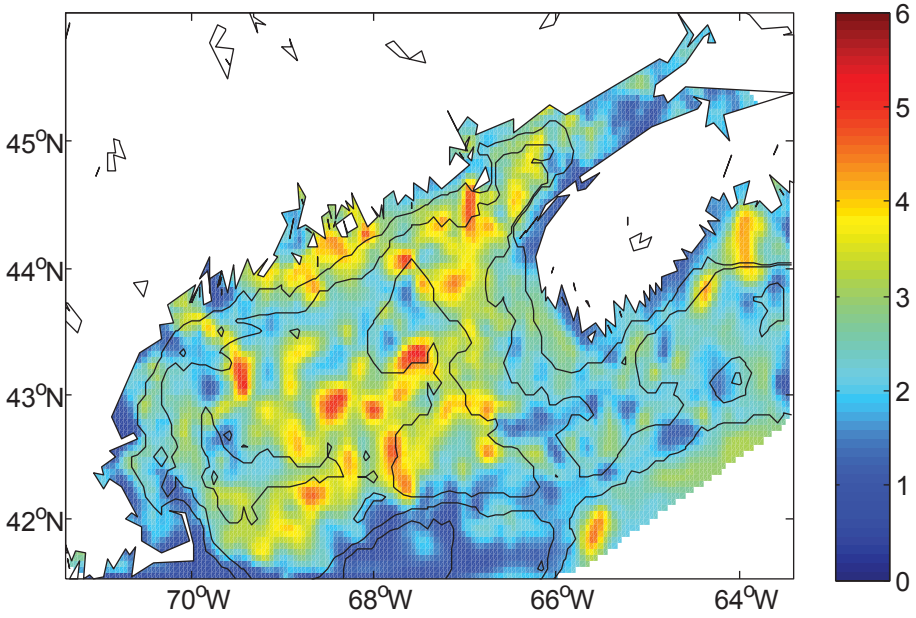

Figure 3.16: Same description as for Figure 3.3a, but with observed sorting (on ϕ scale) instead of mean phi size.

Better sorted sediments characterize the eastern lower of Bay of Fundy, and the western lower Bay of Fundy exhibits less sorted sediments (Figure 3.16). Better sorted sediments also characterize the upper Bay of Fundy with values around $\sim 2.5\ \phi$ in the Minas Passage and Channel, Chignecto Bay, the Avon River's mouth and the Southern Bight of the upper Bay of Fundy.

3.4 Predicted Impact of Potential Tidal Power

Assuming the bed texture is in equilibrium with near-bed hydrodynamics is a simple approach to predicting the impact of tidal power on sediment texture. Figure 3.18 shows the predicted impact on competent mean phi size in the Bay of Fundy and Gulf of Maine. Figure 3.19 is a close-up of the predicted impact on competent mean phi size in Minas Basin. Impact is defined as the difference between present-day and impacted competent mean phi sizes. This approach assumes that if tidal bed shear stress changes, everything else being equal, sediment texture will change accordingly. Competent mean phi sizes are computed using maximum modeled bed bed shear stress, and values of τ_c estimated with the model of *Wiberg and Smith* (1987). Tidal power development scenarios would extract tidal flow (kinetic) energy in the Minas Passage. The 3-D tidal flows for these scenarios were produced by *Hasegawa et al.* (2011). The location of the in-stream turbine array is shown in Figure 3.17. The scenarios of Figures 3.18a and b would produce 7.6 and 2.0 GW of power, respectively. The 7.6-GW and 2.0-GW scenarios are the maximum time-mean (averaged over the model simulation period, i.e. $\sim$ 30 d) amount of power that could potentially be produced by two types of array configuration. The energy extraction would take place over the entire water column in the 7.6-GW scenario, and over the first 20 m above the seabed in the 2.0-GW scenario. Because the 7.6-GW scenario takes place over the entire water column, it can be likened to the impact a tidal barrage would have. Tidal turbines with 1-MW generating capacity can have diameters of up to 20 m (*FORCE*, 2012). Therefore, the 2.0-GW scenario can be likened to the impact a turbine farm would have. An amount of 2.0 GW of power generation at maximum power generation capacity of 1 MW per turbine, which is typical of turbines with 20 m diameters (*FORCE*, 2012), would represent 2000 turbines in the Bay of Fundy.

For the 7.6-GW tidal energy extraction scenario, the biggest impact on competent mean phi size is predicted along the Avon River estuary's coasts and in some small localized areas ($\sim$ 2 km^2) of the Minas Passage, and in Cape Cod Bay. Figure 3.18a shows that larger competent mean phi sizes from 2–5 ϕ are predicted in the Avon River estuary and in the Southern Bight of the Minas Basin. A general increase in competent mean phi sizes between 1–2 ϕ is predicted for the Minas Channel and Basin, but a decrease of down to $\sim$ -2 ϕ is also predicted along the Minas Passage's coasts (Figure 3.19a). An increase in competent mean phi sizes between 1–2 ϕ is predicted northeast of Grand Manan Island,

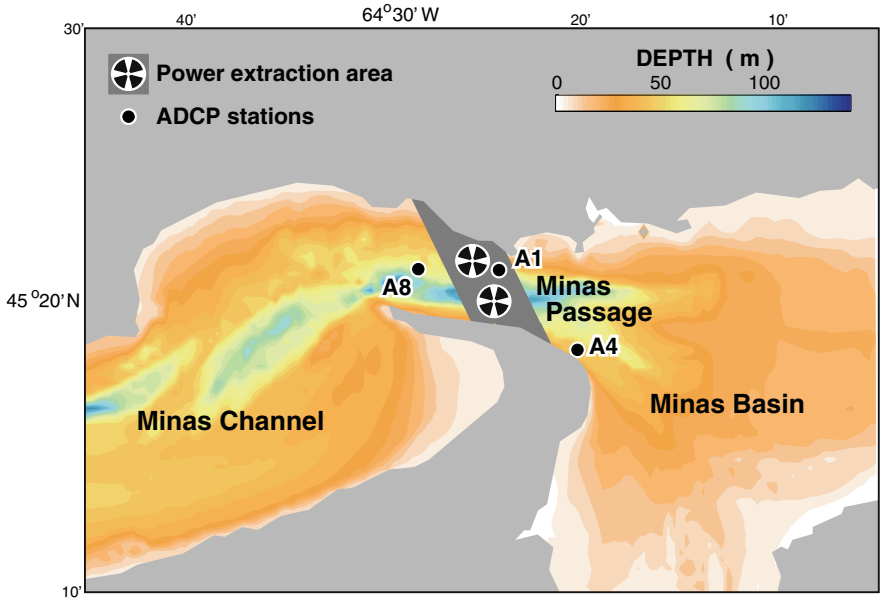

Figure 3.17: Location of in-stream turbine array in the Minas Passage. The location is used in simulations by *Hasegawa et al.* (2011) of the impact of tidal power on tidal circulation in the Bay of Fundy and Gulf of Maine.

and an increase in competent mean phi sizes on the order of 1 ϕ is predicted in most of the Bay of Fundy.

In the Gulf of Maine, no impact to a small increase in competent mean phi sizes, between 0–(-1), is predicted for most of the Gulf of Maine. On the other hand, a decrease in competent mean phi sizes from (-2)–(-1) ϕ is predicted in a few locations, namely the outer Penobscot Bay, parts of Georges and Murray Basins, and in most of Cape Cod Bay and on Stellwagen Bank, and surroundings. Along Maine's coast, an increase in competent mean phi sizes between 0–1 ϕ is predicted.

Figure 3.18b and Figure 3.19b show that the 2.0-GW tidal energy extraction scenario's biggest predicted impact is in the Minas Passage. Larger competent mean phi sizes (than at present) between 1–2 ϕ are predicted in most of the Minas Passage. This is comparable to the impact predicted for most of the Minas Channel and Basin, and northeast of Grand Manan Island in the 7.6-GW scenario. Smaller increases in competent mean phi sizes around $\sim$ 1 ϕ are also predicted northeast of Grand Manan Island and along the Avon River estuary's coasts.

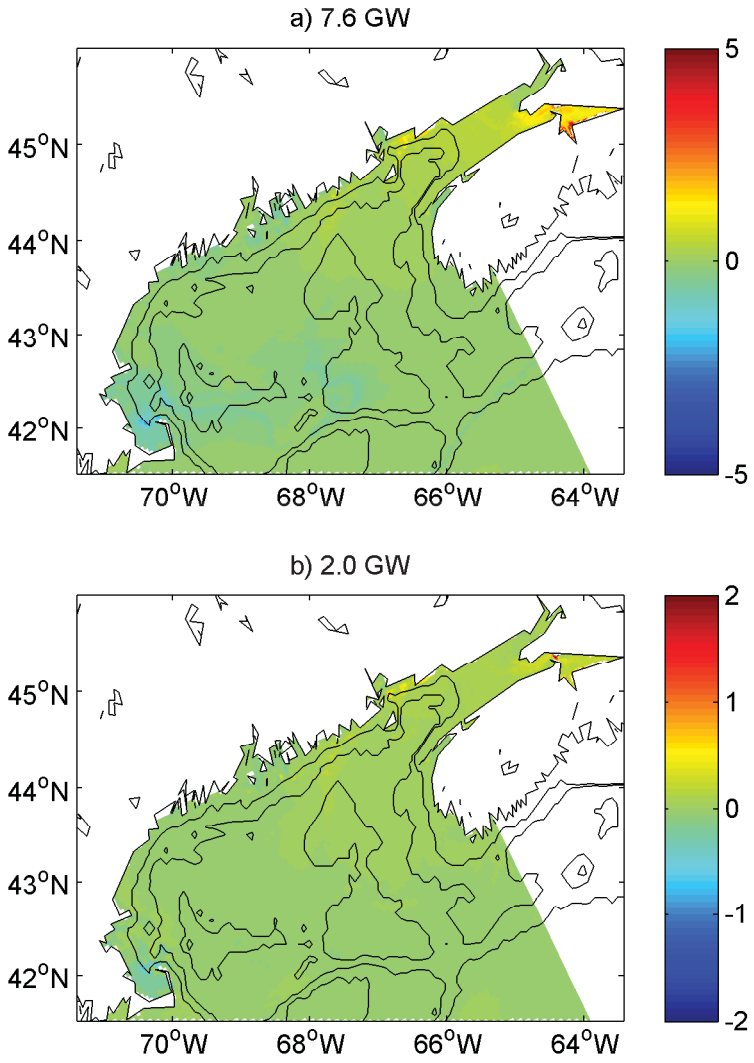

Figure 3.18: Map of impact ($\Delta\phi$) on competent mean phi size for a) 7.6-GW and b) 2.0-GW tidal power development scenarios in the Bay of Fundy and Gulf of Maine region. Impact is defined as the difference between present-day and impacted competent mean phi sizes. Positive values mean a fining of sediments while negative values, a coarsening of sediments.

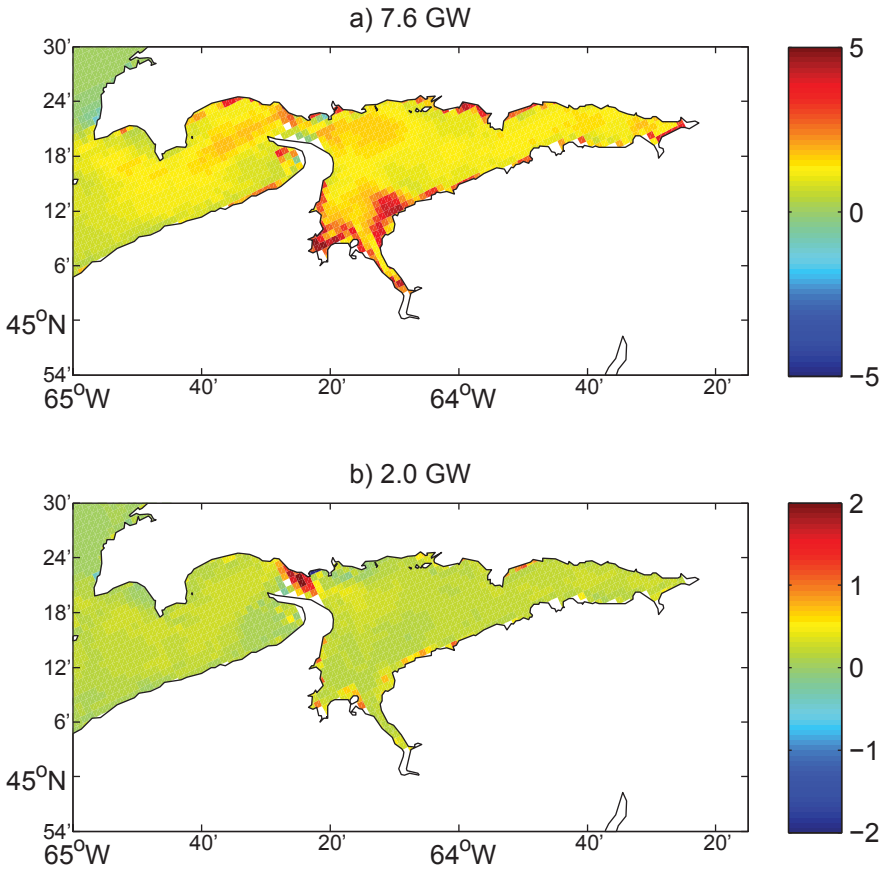

Figure 3.19: Map of impact on competent mean phi size for a) 7.6-GW and b) 2.0-GW tidal power development scenarios in the Minas Basin region. Impact is defined as the difference between present-day and impacted competent mean phi sizes. Positive values mean a fining of sediments while negative values, a coarsening of sediments.

CHAPTER 4

DISCUSSION

4.1 Over-Predicted Competent Mean Grain Sizes

In general, sediment texture is closer to equilibrium with near-bed tidal currents in the Gulf of Maine than in the Bay of Fundy. Contrary to the Bay of Fundy, mean phi size, clay, silt, sand, and gravel contents behave as expected in the Gulf of Maine, in that finer textural classes in samples decrease with increasing maximum tidal bed shear stress. Observed mean phi size, silt, clay and sand content medians generally decrease with increasing maximum modeled tidal bed shear stress in the Gulf of Maine, while gravel content medians generally increase with increasing maximum tidal bed shear stress. In the Bay of Fundy, no such trends were found between mean phi size, silt, clay, sand and gravel content and maximum tidal bead shear stress. There is better agreement between competent and observed mean phi sizes in the Gulf of Maine than in the Bay of Fundy. While most values of ϵ_M are < 4 in the Gulf of Maine, these are > 4 in the Bay of Fundy (Figure 3.10). There is better correlation between competent and observed mean phi sizes in the Gulf of Maine than in the Bay of Fundy. While values of R^2 reach ~ 0.8 in the Gulf of Maine, all values are < 0.1 in the Bay of Fundy (Figure 3.8).

4.2 Missing Dynamics and Processes

Flows induced by waves and baroclinicity, and unresolved processes in the ocean circulation model, could explain the general disagreement, and lack of correlation, between observed and competent mean phi sizes.

4.2.1 Wave-Induced Bed Shear Stress

Wave-induced bed shear stresses are generally of marginal geographical importance in the Bay of Fundy and Gulf of Maine. Wave-generated bed shear stresses can resuspend sediments and facilitate subsequent transport by near-bed tidal currents for instance. These can also enhance bed shear stress when occurring at the same time as current-induced bed shear stress (*Grant and Madsen*, 1979). This study has not investigated this source of bed shear stress. There is evidence in other studies, in the Bay of Fundy and Gulf of Maine region, and elsewhere, that these are a significant source of bed shear stress only in shallow regions of the coastal environment. *Li* (2011) noted that in the Bay of Fundy, wave-generated bed shear stresses play a minor role in the distribution of sediments, except for shallow coastal areas. *Amos and Judge* (1991) noted that tides dominate sediment transport even on shallow parts, i.e. depths < 120 m, of banks in the Gulf of Maine.

4.2.2 Baroclinicity-Induced Bed Shear Stress

Baroclinicity-generated bed shear stresses represent another source of bed shear stress that can potentially be of importance for the distribution of sediments. A baroclinic fluid is one where lines of constant pressure cross lines of constant density. For instance, differences in mixing in the horizontal of an ocean domain can produce this situation. This generates additional near-bed momentum, and consequently bed shear stress. Baroclinicity-generated bed shear stresses have not been investigated in this thesis. Few studies have investigated the role of this source of bed shear stress on the distribution of sediments. *Signell et al.* (2000) found that in Long Island Sound, simulated baroclinicity-driven speeds 1 m above the seabed could reach 6–8 cm s^{-1}. These last authors estimated that in Long Island Sound, baroclinicity-driven near-bed currents play a minor role in the distribution of sediments. In the Gulf of Maine, *Xue et al.* (2000) forced an ocean circulation model with monthly climatological wind and heat flux to find that monthly-averaged velocities at a depth of 100 m were generally well < 20 cm s^{-1}. The highest values found by these last authors are notably offshore of Maine's coast. This is more or less where modeled maximum tidal speeds 1 m above the seabed in the present study are lowest. In the Bay of Fundy, *Aretxabaleta et al.* (2008) modeled depth-averaged baroclinic current speeds of ~ 5 cm s^{-1} east of Grand Manan Island for the months of May and June. Generally, modeled maximum tidal speeds 1 m above the seabed in the present study are well > 10 cm s^{-1} for that region (Figure 3.1). Well-mixed waters also characterize most of the Bay of Fundy for

times of the year (July and August) when thermal stratification would be expected to occur (*Garrett et al.*, 1978). Well-mixed waters and the small magnitude of baroclinic flows limit potential interactions with tidal flows that could act to reduce maximum bed shear stresses the seabed experiences.

4.2.3 Unresolved Processes

Other unresolved processes should not lead to a systematic over-estimation of tidal bed shear stresses in the Bay of Fundy relative to the Gulf of Maine. The circulation model used in this study has a value constant value of roughness length, z_0 = 0.01 m, which would be more suited to coarse-grained sedimentary environments. This could lead to better estimation of tidal bed stresses in coarse-grained environments. Figure 4.1 shows R^2 values as a function of observed mean phi size for the Bay of Fundy and Gulf of Maine. R^2 values are that of Figure 3.11 and mean phi size is an average of observations in each cell of the same figure. Higher correlation is not found in regions of coarser mean phi sizes, as no clear trend can be observed in Figure 4.1. In addition, as a simplification of reality, the numerical ocean circulation has an associated margin of error. Nonetheless, validation against observations was done for the model used in this study (*Hasegawa et al.*, 2011). Validation ensures that predictions are reasonably consistent with observations. In an area as big as the Bay of Fundy and Gulf of Maine, on the other hand, modeling is a challenge. Thus, choices have to be made such as the $\sim$ 1.5–4.5-km resolution of the present study's circulation model. This choice is a simplification of reality, and consequently, small features of ocean circulation due to bed roughness can not be always be modeled accurately. Most importantly, the sediment samples depend on these small features of ocean circulation. This should not lead to a systematic over-estimation of bed shear stresses only in the Bay of Fundy. *Fader et al.* (1977) noted that east of Grand Manan Island, fine sediments are consolidated. There may be over-consolidated fine sediments elsewhere in the Bay of Fundy. The τ_c model of *Wiberg and Smith* (1987) does not account for this consolidation of sediments, and would under-estimate the value of τ_c for sediments in the region. While fine sediments represent about a half of all observations in the Bay of Fundy (Figure 3.3), the remainder is mostly in the sand range and the over-consolidation does not apply to those. The limitations of the *Wiberg and Smith* (1987) critical erosion shear stress model generally should not affect the estimation of competent mean phi sizes in this study. The model of *Wiberg and Smith* (1987) agrees well with observations in the

fine sand to coarse gravel range, i.e. 4-(-4). The τ_c values for these textural classes are $\sim$ 0.1 and 10 Pa, respectively. Modeled bed shear stresses only fall below 0.1 Pa at a few sediment sample locations in the Bay of Fundy and Gulf of Maine, and do not reach 10 Pa at all sample locations (Figures 3.3b and c).

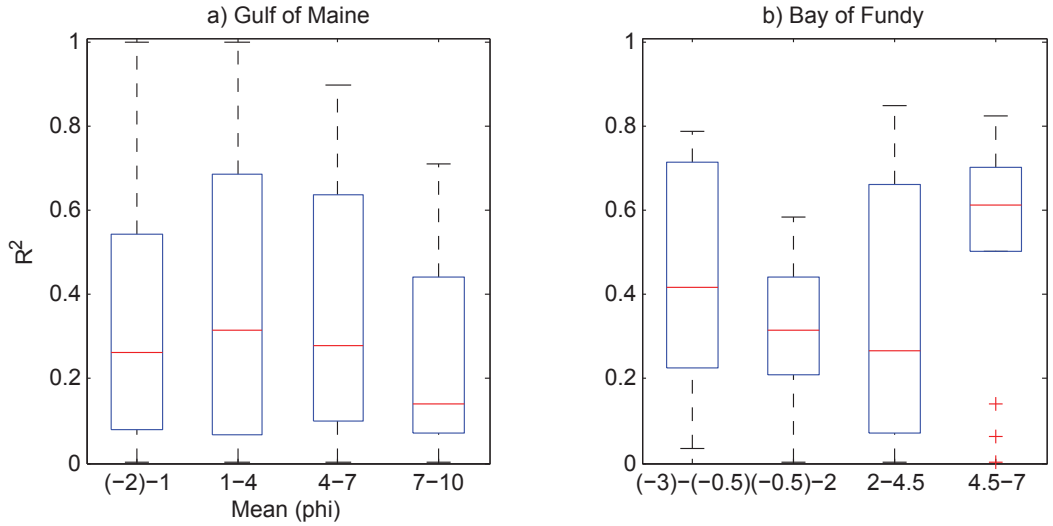

Figure 4.1: Boxplots of observed mean phi size versus R^2 between 1-ϕ bin-averaged observed and competent mean phi sizes for the a) Gulf of Maine and b) Bay of Fundy region. The boxes' upper and lower edges represent the first and third quartiles, respectively, while the boxes' middle lines represent the median of data. The whiskers represent the lowest and highest values within 1.5 times the respective interquartile distances. Crosses represent outliers.

Sampling-related errors should also not lead to a systematic bias in mean grain size of the samples of the Bay of Fundy. These errors contribute to scatter in data that is observed, but should not influence observed trends in the Bay of Fundy more than in Gulf of Maine. The observed mean phi sizes in the Bay of Fundy and Gulf of Maine (Figure 3.3) come from data bases and data sets with many sampling periods, and analysis methods. Furthermore, modern methods of grain size analysis such as the Coulter counter also have a margin of error.

4.3 Competent Grain Size in the Ocean

A competent grain size approach is expected to work under a set of conditions. The good agreement between observed and competent mean phi sizes in Figure 3.10 depends on the respect of assumptions used in making predictions. In the Bay of Fundy and Gulf of Maine, the competent mean grain size predicted with the barotropic model should approximate observed mean grain size when: barotropic tidal near-bed currents are the dominant source of bed shear stress, sediment supply of grain sizes smaller than competence of near-bed flow does not exceed transport capacity of the near-bed flow, all grain sizes are resuspended under the maximum bed shear stress, and a residual near-bed current is present to carry away resuspended particles. If there is no residual tidal near-bed flow, resuspended sediments will deposit at their original location of resuspension.

4.3.1 Assumptions in the Bay of Fundy

One might expect the assumptions for competent mean grain sizes to approximate observed mean grain sizes to be satisfied in the Bay of Fundy. First, there is a variety of grain sizes present in the Bay of Fundy, and those are potentially in transport frequently. It was found that the estimated critical erosion erosion shear stress of fine silt was exceeded by modeled tidal bed shear stresses close to a 100 % of the time for almost the entire Bay of Fundy and Gulf of Maine (Figure 3.15a). Fine sand is potentially resuspended by near-bed tidal currents most of the time ($>$ 50 %) in most of the Bay of Fundy. Fine gravel is potentially resuspended by near-bed tidal currents most of the time in most of the Minas Channel and the central Minas Basin in the Bay of Fundy. These results are consistent with those of *Li et al.* (2010) for the Bay of Fundy and Scotian Shelf. Second, there is wide-spread presence of residual near-bed tidal flow in the Bay of Fundy. As a proxy for residual near-bed flow, residual modeled tidal bed shear stress magnitude for the Bay of Fundy and Gulf of Maine is shown in Figure 3.14. Third, sediment supply is apparently limited as rivers do not discharge much sediment into the Bay of Fundy, contributing only an estimated 5.9×10^4 m^3 a^{-1}. Locally, rivers that supply fine and coarse material to the coasts of the Gulf of Maine and Bay of Fundy may influence sediment texture. Other studies such as that of *Emery and Uchupi* (1972) noted that along the coast of Maine and in Passamaquoddy Bay, the source of sands is mainly fluvial. *Fader et al.* (1977) noted that the St. John River contributes a substantial amount of fines to the adjacent accumulation of fines east

of Grand Manan Island. Overall, however, fluvial sediment supply is small.

4.3.2 Sediment Supply in the Bay of Fundy

An absence of residual flow in the Bay of Fundy is not the cause for disagreement and lower correlation between observed and competent grain sizes in the Bay of Fundy. It is hypothesized that the stronger the near-bed tidal flow is, the higher the agreement and correlation should be, as stronger near-bed tidal flows transport resuspended material from its site of erosion. Figure 4.2 shows R^2 values as a function of the magnitude of residual modeled tidal bed shear stress for the Bay of Fundy and Gulf of Maine. Generally, Figure 4.2b shows that as residual bed shear stress increases, R^2 median values decrease in the Bay of Fundy, and the contrary generally happens in the Gulf of Maine.

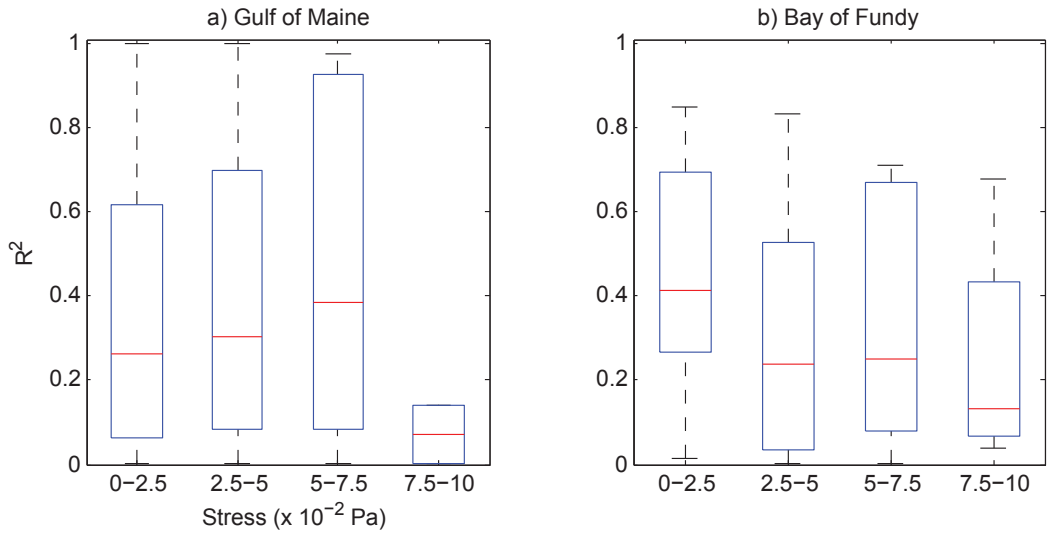

Figure 4.2: Boxplots of magnitude of residual modeled tidal bed shear stress versus R^2 between 1-ϕ bin-averaged observed and competent mean phi sizes for the a) Gulf of Maine and b) Bay of Fundy region. For the boxplots, the description is the same as for Figure 4.1.

Frequent transport of sand is not the cause of disagreement and lower correlation between observed and competent grain sizes in the Bay of Fundy. Sand is widespread in the Bay of Fundy (Figure 3.5); hence, its frequent resuspension is hypothesized to be necessary for the bed to equilibrate with maximum tidal bed shear stress. Figure 4.3 shows R^2 values as a function of the % of time τ_c of fine sand is exceeded by the magnitude of

modeled tidal bed shear stress for the Bay of Fundy and Gulf of Maine. Figure 4.3a shows that R^2 median values generally decrease as the % of time τ_c of fine sand is exceeded by modeled bed shear stresses increases in the Bay of Fundy, and the contrary generally happens in the Gulf of Maine.

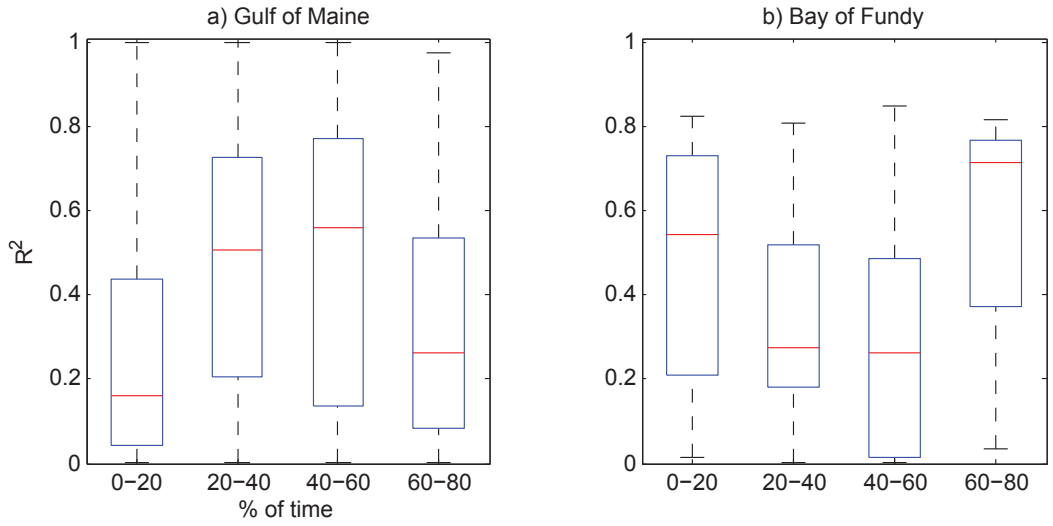

Figure 4.3: Boxplots of the % of time τ_c of fine sand is exceeded by the magnitude of modeled tidal bed shear stress versus R^2 between 1-ϕ bin-averaged observed and competent mean phi sizes for the a) Gulf of Maine and b) Bay of Fundy region. For the boxplots, the description is the same as for Figure 4.1.

It is possible that sediment supply is the source of disagreement between observed and competent mean phi sizes, but the sediment is not fluvial in origin. There is an abundant supply of sediment from the erosion of adjacent cliffs in the Bay of Fundy. *Amos and Long* (1980) estimated that the Minas Basin alone receives each year 4.8×10^6 m^3 of material from different sources. 58 % of this material enters the Minas Basin as sand, 35 % as silt and clay, 7 % as material bigger than sand. The biggest source of material is the erosion of adjacent cliffs, mainly made out of sandstone, at a rate of 2.72×10^6 m^3 a^{-1} (supply from rivers is 1.91 % of supply from cliff erosion). Sandstone cliffs also represent a large fraction of the northern coastline in the remainder of the Bay of Fundy. Therefore, in the Bay of Fundy, sediment supply from erosion of adjacent cliffs likely is the cause of competent mean grain sizes being coarser than observed mean grain sizes. When there

is a high input of sediment smaller than the competent grain size, observed sediment texture is expected to be finer than the competence of flow would predict. *Buffington and Montgomery* (1999) found that in gravel-bed rivers with high sediment supply finer than competent grain size, competent median grain sizes tend to be larger than observed median grain sizes. Consistent with the previous finding, the panels of Figure 3.8 show predicted mean phi sizes that are generally smaller than observed mean phi sizes. Also, these range from (-6)-ϕ gravel to 9-ϕ clay, which is similar to the composition of material originating from cliffs adjacent to the Bay of Fundy. In addition, *Lambiase* (1980) found that maximum bed shear stress is not a good predictor of coarsest grain size in the Avon River estuary because of the abundant fine material supply. Other sources also supply fine material to the Bay of Fundy. *Fader et al.* (1977) observed that the Scotian Shelf Drift in the Gulf of Maine and Bay of Fundy had been winnowed of its fine material. He additionally noted that a surface cyclonic gyre was present over much of year in the western lower Bay of Fundy. This finding was recently confirmed by *Aretxabaleta et al.* (2008). *Fader et al.* (1977) noted that the observed residual circulation in the lower Bay Fundy was important for fine-grained sediment transport. When the residual circulation forms a closed gyre, like in the western lower Bay of Fundy, fine sediment could potentially be retained, and make competent grain sizes coarser than observed grain sizes.

The large sand body in the eastern lower Bay of Fundy is additional evidence of sand supply to this region. This would further support the hypothesis that an abundant supply of sand is the explanation for low correlations and agreements calculated in the Bay of Fundy (Figure 3.8 and Figure 3.10, respectively). Sand that is frequently in transport because of high tidal bed shear stresses, and the transport convergence in the region could explain the high observed sand contents (Figure 3.5). West of the Minas Channel, there is a westward convergence of residual modeled tidal bed shear stress vectors because these generally decrease in magnitude. In addition, sand is potentially frequently resuspended in the region. The % of time the τ_c of fine sand is exceeded by the magnitude of modeled tidal bed shear stresses is mostly between 60 and 100 % in the Bay of Fundy (Figure 3.15b). More recently, *Wu et al.* (2011) calculated that bedload sediment transport formed a counter-clockwise gyre in the western Minas Channel. Sandwaves have been confirmed to move west in the north of Scots Bay, and to the east in the south, by observational studies. West of the Minas Channel, in the lower eastern Bay of Fundy, trapped sandwaves have also been observed

(*Parrott et al.*, 2008). According to an interpretation of the findings of *Lambiase* (1980), competent grain sizes should eventually reach the area and this would cause the bed to equilibrate with near-bed flow. Fine gravel has been estimated to be in transport between 40 and 100 % of the time in the upper Bay of Fundy (Figure 3.15c). If fine gravel moves slower as bedload than fine sand, it should arrive after and cover the sand. But *Amos and Long* (1980) has estimated that most of material that enters the Minas Basin on an annual basis is sand. This is probably why large sand contents are found in the lower eastern Bay of Fundy, even though material coarser than sand probably reaches the area.

4.4 Implications

In the Bay of the Fundy, tides dominate sediment transport (*Amos and Judge*, 1991; *Fader et al.*, 1977; *Li et al.*, 2010; *Emery and Uchupi*, 1972; *Wu et al.*, 2011), but they likely do not dominate texture. This means that future efforts to model sediment texture in the Bay of Fundy will need to include supply from adjacent cliffs.

Now, knowledge gained in the present thesis can help to assess predicted impacts of potential tidal power development in Bay of Fundy on sediment texture (Figure 3.18). For the Bay of Fundy, without further modeling that would include supply, it can be reasonably said that the impact should be small because sediment supply likely dominates texture. For the Gulf of Maine, the predicted impact needs to be assessed with more detail than the Bay of Fundy as the equilibrium assumption is generally more applicable. In the Gulf of Maine, the predicted coarsening and fining in Cape Cod Bay and northeast of Grand Manan Island, respectively, should be impacts of the 7.6-GW tidal energy extraction scenario (Figure 3.18a). This is because some correlation was found between observed an predicted mean phi sizes in these regions (Figure 3.8). On the other hand, a coarsening between $\sim$ (-2)–(-1) ϕ (a change in texture from silt to fine sand for a -2 ϕ coarsening west of Cape Cod) in Cape Cod Bay is more certain than a fining between $\sim$ 1–2 ϕ northeast of Grand Manan Island. This is because of low agreements between observed and predicted mean phi sizes northeast of Grand Manan Island in Figure 3.10. These low agreements have been hypothesized to be caused by fluvial and possibly other sediment supply influences on sediment texture in the area. For the remainder of the Gulf of Maine, on the other hand, predicted impacts of the 7-6 GW scenario should be negligible. This is mainly because of the small magnitude of predicted impacts, even though high correlations and

agreements have been calculated for certain regions of the Gulf of Maine. Along Maine's coast, statistically non-significant correlations make the predictions very uncertain.

CHAPTER 5

CONCLUSION

This thesis has shown that generally in the Gulf of Maine, sediment texture is closer to equilibrium with maximum conditions of tidal near-bed currents than in the Bay of Fundy. Medians of mean grain size and gravel content increase, and silt, clay, and sand content generally decrease with increasing maximum modeled tidal bed shear stress in this region. Competent mean grain sizes estimated with maximum modeled tidal bed shear stress in the Gulf of Maine are generally in closer agreement with observed mean grain sizes than in the Bay of Fundy. Georges Bank and the Scotian Slope are regions where competent mean grain sizes approximate observed mean grain sizes with precision.

Sediment texture is likely dominated by supply in the Bay of Fundy. In the Bay of Fundy, mean grain size is generally further out of equilibrium with maximum tidal bed shear stress than in the Gulf of Maine. In the Minas Basin, this supply is mainly sand from adjacent erosion of cliffs (*Amos and Long*, 1980).

Many limitations characterize the approach of the present thesis, but differences in sediment texture controls between the Bay of Fundy and Gulf of Maine have still emerged. Other sources of bed shear stress such as baroclinicity- and wave-generated bed shear stresses, which might influence sediment texture in marginal areas of the Bay of Fundy and Gulf of Maine, have not been included. The main limitation of this study is the discrepancy between the spatial resolution of the ocean circulation model and the sediment data. Sediment samples' texture depend on hydrodynamic processes that occur at smaller scales than that of the ocean circulation model.

Knowledge gained in this thesis has enabled an assessment of the impact of two tidal power development scenarios. Great potential for tidal power development has been

estimated for the Minas Passage, Bay of Fundy (*Hasegawa et al.*, 2011). However, this development could have adverse effects on the physical environment of the Bay of Fundy and Gulf of Maine. In the entire Bay of Fundy, sediment supply has been shown to dominantly influence texture, and smaller impact than predicted in this thesis can be reasonably expected whatever the extent of future development, i.e. < 7.8 GW. Furthermore, the impact assessment in the Gulf of Maine involves a lot of uncertainty. This is mainly because of the poor agreements between observed and predicted mean phi sizes, but also because of assumptions made for the prediction of the impact. For a 7.6-GW tidal power development scenario, a coarsening should occur in most of Cape Cod Bay.

5.1 Future Work

Results from the present thesis make it clear that future modeling efforts will need to include the influence of sediment supply from adjacent cliffs in the Bay of Fundy. Morphodynamic modeling would likely be useful on the smaller scale of a turbine array, but also in the entire Bay of Fundy. A potential change in sediment texture does not provide information on the impact tidal power development might have on seabed morphology, and navigability. Prior work in the Gulf of Maine has established that seabed morphology changes over long time scales (50 m clay accumulation in the basins of the Gulf of Maine in 10 kyr (*Emery and Uchupi*, 1972)). Tidal power development should shorten these time scales. For comparison, *Neill et al.* (2011) predicted that a 300-MW tidal in-stream turbine array could impact erosion and deposition by as much as 10 % over a spring-neap tidal cycle within a radius of ~ 10 km.

In the lower eastern Bay of Fundy, residual near-bed circulation has been hypothesized to explain the higher sand contents by moving the abundant supply from adjacent cliffs in the Minas Basin. An experiment that would confirm this is a virtual release of particles in the model simulated near-bed flow field. On the other hand, this would not completely solve the problem. This is because sediment particles in suspension (or as bedload) usually deposit when there is transport convergence, or bed shear stresses are not strong enough to keep them so. Convergence is hypothesized to cause the deposition of sand. Therefore, a sediment transport model coupled to a tidal circulation model is likely needed to fully address the hypothesis. *Hasegawa et al.* (2011) have shown that a 7.8-GW tidal power development scenario in the Minas Passage would impact residual tidal circulation in its

vicinity. For a 2.0-GW tidal power development scenario, they have shown that the impact would be small (compared to the 7.8-GW scenario). Therefore, if convergence of residual tidal circulation in the eastern lower Bay of Fundy is responsible for the accumulation of sand, small impact for sand accumulation rates should be expected from more realistic tidal power development, i.e. $<$ 2.0 GW.

Potential changes in sediment texture could affect benthic plant and animal species. The present thesis has not examined the potential consequences for species that inhabit the area's seabed at the moment. For example, future work could examine present species' sensitivity to changing habitat conditions and colonization by other species of newly suitable habitats.

Including other sources of bed shear stress in the calculation of maximum hydrodynamic conditions could lead to further findings as to the observed sediment texture. Other sources of bed shear stress, such as storm-generated waves, have not been examined in this thesis. It is generally accepted that waves have an influence on sediment texture in marginal, coastal areas in the the Bay of Fundy and Gulf of Maine (*Amos and Judge*, 1991; *Li*, 2011). On the other hand, tidal power development will most likely not affect wave characteristics in the Bay of Fundy and Gulf of Maine. It is more on interactions of wave- and tidal current-generated bed shear stresses that tidal power development could have further impact on sediment texture. But these changes in interactions should be very small, as the impact on texture from potential large-scale tidal power should be small in the Gulf of Maine.

APPENDIX A

CRITICAL EROSION SHEAR STRESS MODEL

The following theoretical derivation of the non-dimensional critical erosion shear stress, $\tau_c^\star$, is taken from *Wiberg and Smith* (1987). Figure A.1 shows the graphical representation used by *Wiberg and Smith* (1987) to derive $\tau_c^\star$.

The immersed weight of the grain is

$$F_g^{'} = F_g - F_B = (\rho_s - \rho)gV, \tag{A.1}$$

where F_g is the weight of the sediment grain, F_B is the buoyancy force, ρ_s is the grain density, ρ is the seawater density, g is the gravitational acceleration, and V is grain volume.

The drag force is

$$F_D = \frac{1}{2}\rho C_D < u^2(z) > A_x, \tag{A.2}$$

where C_D is the drag coefficient, $< u^2(z) >$ is the grain height-averaged velocity squared, i.e. $(1/D)\int_0^D u^2(z)dz$, and A_x is the grain cross-sectional area. C_D depends on the particle Reynolds number, $R_\star =< u > D/\nu$, where D is the grain diameter and ν is the seawater kinematic viscosity.

Furthermore, using a scaling of bed shear stress $\tau_0 = \rho u_\star^2$, involving the friction velocity $u_\star$, and assuming the grain cross-sectional velocity profile is of the following form: $u(z) = u_\star f(z/z_0)$, Equation A.2 is equivalent to

$$F_D = \frac{1}{2}\rho C_D \tau_0 < f^2(z/z_0) > A_x, \tag{A.3}$$

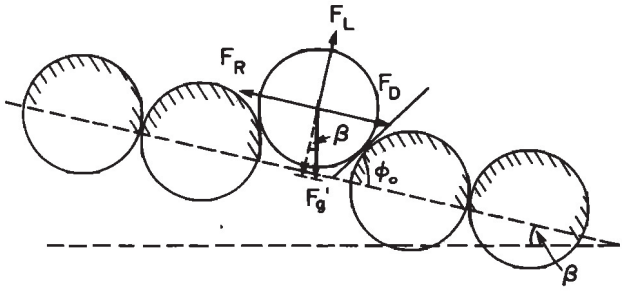

Figure A.1: Schematic of a sediment grain under the action of the forces involved in motion incipiency (*Wiberg and Smith*, 1987).

where z is the vertical Cartesian coordinate (from the seabed) and z_0 is the roughness parameter.

The lift force is

$$F_L = \frac{1}{2}\rho C_L (u_T^2 - u_B^2) A_x \tag{A.4}$$

or

$$F_L = \frac{1}{2}\rho C_L \tau_0 [f^2(z_T/z_0) - f^2(z_B/z_0)] A_x, \tag{A.5}$$

where subscripts T and B represent top and bottom, respectively, and C_L is the lift coefficient.

The friction force, or resistive force, is

$$F_R = F_N \tan\phi_0, \tag{A.6}$$

where F_N is the normal force and ϕ_0 is the angle of repose, or steepest angle the grain can withstand before sliding. Note that $\tan(\phi_0)$ is analogous to the static friction coefficient, μ_S. Furthermore, as F_N can be calculated from $F_g^{'}$ and F_L, Equation A.6 is equivalent to

$$F_R = (F_g^{'} \cos\beta - F_L) \tan\phi_0, \tag{A.7}$$

where β is the seabed inclination.

Summing the forces in the horizontal at incipient motion, denoted by subscript c, yields

$$\Sigma F_H = 0 = (F_g^{'} \cos\beta - F_L)\tan\phi_0 = F_D + F_g^{'} \sin\beta \tag{A.8}$$

and substituting Equations A.3 and A.5 in Equation A.8, and multiplying the latter equation by D/D, yields the dimensionless critical erosion shear stress

$$\tau_c^{\star} = \frac{2}{C_c^D \alpha} \frac{1}{< f^2(z/z_0) >} \frac{tan\phi_0 \cos\beta - \sin\beta}{1 + F_c^L/F_c^D \tan\phi_0}, \tag{A.9}$$

where $\alpha = A_x D/V$, which for a sphere, $\alpha = 1.5$. To obtain Equation A.9, another expression for $\tau_c^{\star}$ was used, which is

$$\tau_c^{\star} = \frac{\tau_c}{(\rho_s - \rho)gD}, \tag{A.10}$$

where τ_c is the critical erosion shear stress.

Furthermore, $< f^2(z/z_0) >$ depends on the bed roughness Reynolds number $R_{\star} = u_{\star}k_s/\nu$, where k_s is the length scale of the bed roughness. For $R_{\star} > 100$, the structure of velocity profile is

$$f^2(z/z_0) = \frac{1}{\kappa}\ln(z/z_0), \tag{A.11}$$

where κ is the Von Kármán constant and $z_0 = k_s/30$.

For $R_{\star} < 3$, the structure of the velocity profile is

$$f^2(z/z_0) = \frac{1}{\kappa}\ln(1 + \kappa z^+) - c(1 - e^{-z^+/11.6} - \frac{z^+}{11.6}e^{-0.33z^+}), \tag{A.12}$$

where $z_0 = \nu/(9u_{\star})$, $z^+ = R_{\star}z/k_s$, $z_0^+ = R_{\star}z_0/k_s$ and $c = \kappa/(\ln(z_0^+) + \ln\kappa) = -7.78$.

For $3 < R_{\star} < 100$, the structure of the velocity profile is of the same form as Equation A.12, but $z_0 = f(R_{\star})k_s$, where the function $f(R_{\star})$ can take values between 0.034–0.03327 depending on the value of $R_{\star}$ (*Smith*, 1977).

The particularity of the expression of *Wiberg and Smith* (1987) for τ_c° is that it allows one to take into account the influence of the bed's roughness, k_s, relative to D. This influence is accounted for through the angle of repose

$$\phi_0 = \cos^{-1}(\frac{D/k_s + z_{\star}}{D/k_s + 1}). \tag{A.13}$$

APPENDIX B

LAW OF THE WALL

The following derivation of the law of the wall, or logarithmic velocity profile, is taken from *Stewart* (2009). Figure B.1 shows the graphical representation used by *Stewart* (2009) to derive the law of the wall.

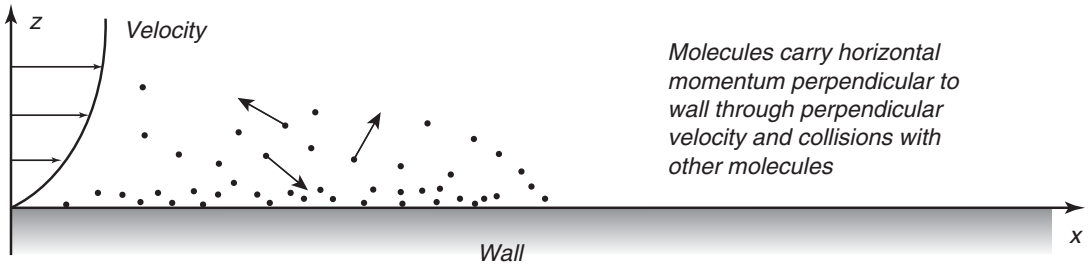

Figure B.1: Graphical representation of a bed sheared by a fluid flow (*Stewart*, 2009).

Using the shear velocity definition, $u_\star = (\tau/\rho)^{1/2}$, in the general shear stress expression, which is

$$\tau(z) = \mu \frac{dU}{dz} \tag{B.1}$$

and substituting the the eddy viscosity A_z for the molecular viscosity μ yields

$$u_\star^2 = A_z \frac{dU}{dz}, \tag{B.2}$$

where U is the instantaneous speed (referred to mean Reynolds-averaged speed in *Stewart* (2009)) the horizontal, ρ is the fluid density and z is the vertical Cartesian coordinate (from the seabed). Equation B.2 is valid away from the seabed where the flow is turbulent, and molecular friction is not important.

Assuming the eddy viscosity, $A_z = \kappa z u_\star$, Equation B.2 becomes

$$u_\star^2 = \kappa z u_\star \frac{dU}{dz}, \tag{B.3}$$

where κ is the Von Kármán constant.

Rearranging Equation B.3 yields

$$\frac{dU}{dz} = \frac{u_\star}{\kappa z} \tag{B.4}$$

and integrating Equation B.4 in z, with the boundary condition $U(z_0/z_0) = 0$ (constant of integration equals zero), yields the law of the wall, which is

$$U(z) = \frac{u_\star}{\kappa} \ln(\frac{z}{z_0}), \tag{B.5}$$

where z_0 is the roughness parameter.

BIBLIOGRAPHY

Allen, G. P., Relationship between grain size parameter distribution and current patterns in the Gironde estuary (France), *Journal of Sedimentary Petrology*, *41*, 74–88, 1971.

Amos, C. L., and J. T. Judge, Sediment transport on the eastern Canadian continental shelf, *Continental Shelf Research*, *11*, 1037–1068, 1991.

Amos, C. L., and B. F. N. Long, *The coastline of Canada*, chap. The sedimentary character of the Minas Basin, Bay of Fundy, pp. 123–152, GSC, 1980.

Aretxabaleta, A. L., D. J. McGillicudy-Jr., K. W. Smith, and D. R. Lynch, Model simulations of the Bay of Fundy Gyre: 1. climatological results, *Journal of Geophysical Research*, *113*, C10027, 2008.

Bethea, R. M., B. S. Duran, and T. L. Boullion, *Statistical Methods for Engineers and Scientists*, Marcel Dekker, Inc., 1995.

Blaas, M., C. Dong, P. Marchesiello, J. C. McWilliams, and K. C. Stolzenbach, Sediment-transport modeling on Southern Californian shelves: a ROMS case study, *Continental Shelf Research*, *27*, 832–853, 2007.

Bobertz, B., and J. Harff, Sediment facies and hydrodynamic setting: a study in the south western Baltic Sea, *Ocean Dynamics*, *54*, 39–48, 2004.

Buffington, J. M., and D. R. Montgomery, A systematic analysis of eight decades of incipient motion studies, with special reference to gravel-bedded rivers, *Water Resources Research*, *33*, 1993–2029, 1997.

Buffington, J. M., and D. R. Montgomery, Effects of sediment supply on surface textures of gravel-bed rivers, *Water Resources Research*, *35*, 3523–3530, 1999.

Deutsch, C. V., Correcting for negative weights in ordinary kriging, *Computers & Geosciences*, *22*, 765–773, 1996.

Dufois, F., P. Garreau, P. L. Hir, and P. Forget, Wave- and current-induced bottom shear stress distribution in the Gulf of Lions, *Continental Shelf Research*, *28*, 1920–1934, 2008.

Emery, K. O., and E. Uchupi, *Western North Atlantic Ocean: Topography, Rocks, Structure, Water, Life, and Sediments*, The American Association of Petroleum Geologists, 1972.

Fader, G. B., L. H. King, and B. MacLean, Surficial geology of the eastern Gulf of Maine and Bay of Fundy, *Tech. Rep. 76-17*, GSC and Canadian Hydrographic Service, 1977, marine Sciences Paper 19.

FORCE, Technology (section): Atlantis / Lockhead Martin / Irving Shipbuilding, 2012.

Garrett, C., Tidal resonance in the Bay of Fundy and Gulf of Maine, *Nature*, *238*, 441–443, 1972.

Garrett, C. J. R., J. R. Keeley, and D. A. Greenberg, Tidal mixing versus thermal stratification in the Bay of Fundy and Gulf of Maine, *Atmosphere-Ocean*, *16*, 403–423, 1978.

Glover, D. M., W. J. Jenkins, and S. C. Doney, *Modeling Methods for Marine Science*, Cambridge University Press, 2011.

Goff, J. A., C. J. Jenkins, and S. J. Williams, Seabed mapping and characterization of seabed variability using usSEABED data base, *Continental Shelf Research*, *28*, 614–633, 2008.

Grant, W. D., and O. S. Madsen, Combined wave and current interaction with a rough bottom, *Journal of Geophysical Research*, *84*, 1797–1808, 1979.

Greenberg, D. A., A numerical model investigation of tidal phenomena in the Bay of Fundy and Gulf of Maine, *Marine Geodesy*, *2*, 161–187, 1979.

Greenberg, D. A., and C. L. Amos, Suspended sediment transport and deposition modeling in the Bay of Fundy, Nova Scotia - a region of potential tidal power development, *Canadian Journal of Fisheries and Aquatic Sciences*, *40*, 20–34, 1981.

Hasegawa, D., J. Sheng, D. Greenberg, and K. Thompson, Far-field effects of tidal energy extraction in the Minas Passage on tidal circulation in the Bay of Fundy and Gulf of Maine using a nested-grid coastal circulation model, *Ocean Dynamics*, *61*, 1845–1868, 2011.

Jewell, P. W., R. F. Stallard, and G. L. Mellor, Numerical studies of bottom shear stress and sediment distribution on the Amazon continental shelf, *Journal of Sedimentary Petrology*, *63*, 734–745, 1993.

Karsten, R., J. M. McMillan, M. J. Lickley, and R. D. Haynes, Assessment of tidal current energy in the Minas Passage, Bay of Fundy, *Journal of Power and Energy*, *222*, 493–507, 2008.

Lambiase, J. J., Hydraulic control on grain-size distributions in a macrotidal estuary, *Sedimentology*, *27*, 433–446, 1980.

Li, M. Z., Modeling sediment mobility in the Bay of Fundy: how strong the currents are and how often sediment gets transported, 2011, Ocean and Ecosystem Science Seminar Series, Bedford Institute of Oceanography, Halifax, Canada.

Li, M. Z., and D. E. Heffler, Continental shelf sediment transport studies in Canada: principle scientific advances and future directions, *Geoscience Canada*, *29*, 53–68, 2002.

Li, M. Z., C. Hannah, C. Tang, W. Perrie, and R. Prescott, Modeling seabed disturbance and sediment mobility on the Canadian Atlantic Shelf, in *Abstracts Volume, Sedimentology at the Foot of the Andes, 18th International Sedimentological Congress*, 2010.

Loring, D. H., Baseline levels of transition and heavy metals in the bottom sediments of the Bay of Fundy, *Proceedings of the Nova Scotia Institute of Science*, *29*, 335–346, 1979.

Loring, D. H., Geochemical factors controlling the accumulation and dispersion of heavy metals in the bay of fundy sediments, *Canadian Journal of Earth Sciences*, *19*, 930–944, 1982.

Mellor, G. L., User's Guide for a 3-D, Primitive Equation, Numerical Ocean Model, 2004.

Methratta, E. T., and J. S. Link, Associations between surficial sediments and groundfish distributions in the Gulf of Maine-Georges Bank region, *North American Journal of Fisheries Management*, *26*, 473–489, 2006.

Miller, M. C., I. N. McCave, and P. D. Komar, Threshold of sediment motion under unidirectional currents, *Sedimentology*, *24*, 507–527, 1977.

Milligan, T. G., Suspended and bottom sediment grain size distribution in Letang Inlet, N. B., October 1990, *Canadian Technical Reports of Hydrography and Ocean Sciences 156*, BIO, Fisheries and Ocean Canada, 1994.

Neill, S. P., E. J. Litt, S. J. Couch, and A. G. Davies, The impact of tidal stream turbines on large scale sediment dynamics, *Renewable Energy*, *34*, 2803–2812, 2009.

Neill, S. P., J. R. Jordan, and S. J. Couch, Impact of tidal energy converter (TEC) arrays on the dynamics of headland sand banks, *Renewable Energy*, *37*, 387–397, 2011.

Parrott, D. R., B. J. Todd, J. Shaw, J. E. H. Clarke, J. Griffin, B. MacGowan, M. Lamplugh, and T. Webster, Integration of multibeam bathymetry and LiDAR surveys of the Bay of Fundy, Canada, in *Proceedings of the Canadian Hydrographic Conference and National Surveyors Conference*, 2008.

Porter-Smith, R., P. T. Harris, O. B. Andersen, R. Colemen, D. Greenslade, and C. J. Jenkins, Classification of the Australian continental shelf based on predicted sediment threshold exceedance from tidal currents and swell waves, *Marine Geology*, *211*, 1–20, 2004.

Reid, J. M., J. A. Reid, C. J. Jenkins, M. E. Hastings, S. J. Williams, and L. J. Poppe, usSEABED: Atlantic Coast offshore surficial sediment data release, *Data Series 118*, USGS, http://pubs.usgs.gov/ds/2005/118/, 2005.

Shields, J. D., Application of the theory of similarity and turbulence research to the bed load movement, *Mitt. Preuss. Vers. Wasser Schiff*, *26*, 5–24, 1936.

Signell, R. P., J. H. List, and A. S. Farris, Bottom currents and sediment transport in Long Island Sound: a modelling study, *Journal of Coastal Research*, *16*, 551–566, 2000.

Smith, D. J., *The Sea, vol. 6*, chap. Modeling of sediment transport on continental shelves, pp. 539–577, Wiley-Interscience, 1977.

Stewart, R. H., Introduction to Physical Oceanography, 2009.

Stow, C. A., J. Jolliff, D. J. McGillicuddy-Jr., S. C. Doney, J. I. Allen, M. A. M. Friedrichs, K. A. Rose, and P. A. Wallhead, Skill assessment for coupled biological/physical models of marine systems, *Journal of Marine Systems*, *76*, 4–15, 2009.

Sucsy, P. V., B. R. Pearce, and V. G. Panchang, Comparison of two- and three-dimensional model simulation of the effect of a tidal barrier on the Gulf of Maine tides, *Journal of Physical Oceanography*, *23*, 1232–1248, 1993.

Todd, B. J., M. Z. Li, and R. Prescott, Bay of Fundy bedform mapping: linking geomorphology with sediment transport models, in *Programme and Abstracts, GeoHab 2010*, 2010.

Twichell, D. C., Bedform distribution and inferred sand transport on Georges Bank, United States Atlantic Continental Shelf, *Sedimentology*, *30*, 695–710, 1983.

Uncles, R. J., Modeling tidal stress, circulation, and mixing in the Bristol Channel as a prerequisite for ecosystem studies, *Canadian Journal of Fisheries and Aquatic Sciences*, *40*, 8–19, 1983.

Veinot, C., Work Term Report, 2010.

Warner, J. C., B. Butman, and P. S. Dalyander, Storm-driven sediment transport in Massachussets Bay, *Continental Shelf Research*, *28*, 257–282, 2008.

Wiberg, P., and D. J. Smith, Calculations of the critical shear stress for motion of uniform and heterogeneous sediments, *Water Resources Research*, *23*, 1471–1480, 1987.

Wu, Y., J. Chaffey, D. A. Greenberg, K. Colbo, and P. C. Smith, Tidally-induced sediment transport patterns in the upper Bay of Fundy: a numerical study, *Continental Shelf Research*, *31*, 2041–2053, 2011.

Xue, H., F. Chai, and N. R. Pettigrew, Model study of the seasonal circulation in the Gulf of Maine, *Journal of Physical Oceanography*, *30*, 1111–1135, 2000.